Proposal for a Solenoidal Spectrometer to Study Reactions with Short-Lived Beams

A. H. Wuosmaa[1], B. B. Back[2], C. J. Lister[2], K. E. Rehm[2], J. P. Schiffer[2], and S. J. Freeman[3]

[1]*Physics Department, Western Michigan University, Kalamazoo, MI 49008-5252*

[2]*Physics Division, Argonne National Laboratory,*

9700 S. Cass Ave, Argonne IL 60439 and

[3]*Department of Physics and Astronomy,*

University of Manchester, Schuster Laboratory,

Brunswick Street, Manchester, M13 9PL, England

(Dated: November 22, 2005)

Abstract

We propose to construct a new type of spectrometer for the study of reactions in inverse kinematics, built around a high-field magnetic solenoid. This device has significant advantages over more conventional approaches to measurements of key reactions, and is essential to the study of short-lived nuclei. The technique is directly applicable to the research programs at ATLAS, at other present accelerators with secondary beams, and the technique is likely to be important at RIA.

I. SUMMARY

A new concept has been developed for simple reactions with radioactive beams. It is ideally adapted to the 'inverse kinematics' regime necessary for nuclear structure studies in an exotic domain of great current interest. The concept is based on a superconducting solenoidal spectrometer with uniform field. The target and detector are both on the solenoid axis in the field with the reaction products bent back to the axis. The target-to-detector distance and the energy of the particles translate into the desired information of excitation energy and center-of-mass angle.

Such a device has a number of attractive features: greatly improved effective resolution, large solid angle, compact detectors and electronics, and easy particle identification. It is well suited to experiments that probe the structure of the exotic nuclei that are currently of high interest: single-nucleon transfer reactions, pair transfer, inelastic scattering, or even knockout reactions.

The device will consist of a 0.5-m bore, and 1.5 m long 5 T superconducting solenoid, similar to the MRI magnets used in hospitals. It will be commissioned, tested and used at ATLAS with secondary short-lived beams. It also has the potential of being moved to other facilities with short-lived secondary beams if such a move is warranted. Construction and use of the device will also provide valuable experience in a technique that is very relevant to the scientific program of RIA.

Contents

II. SCIENTIFIC JUSTIFICATION

The exploration of the structure of nuclei further and further away from the line of stability is the major focus of contemporary nuclear structure research. Beams of such exotic nuclei are becoming increasingly available and at ATLAS, in particular, a number of beams of light nuclei can be produced at present at useful intensities. The short-lived beams accessible at ATLAS are shown in Fig. 1, with the ones that are likely to have sufficient intensities for reaction studies shown in red and green. The few nuclides that have sufficiently long lifetimes to be produced at another accelerator and subsequently be accelerated are shown in blue.

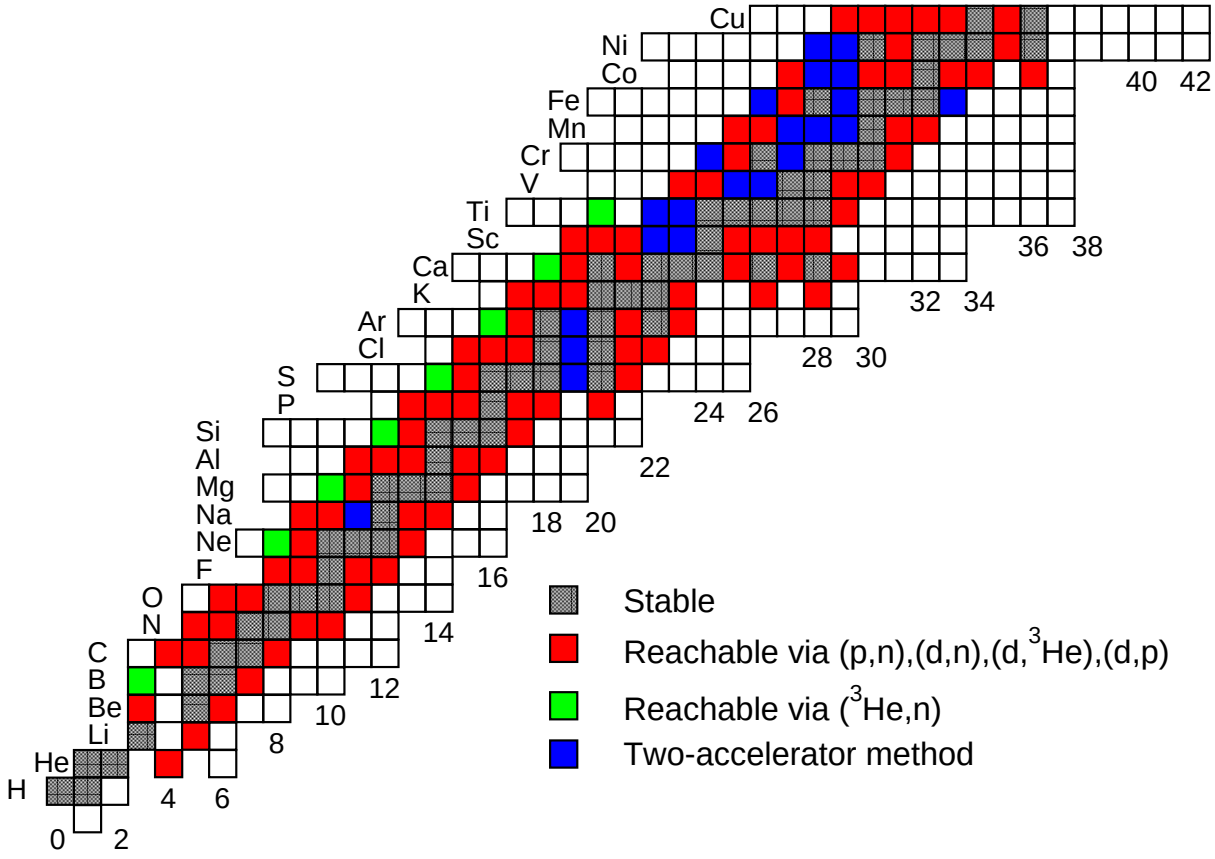

FIG. 1: Radioactive beams presently available or potentially available at the ATLAS facility with those reachable by reactions with high yield shown in red and green. The few nuclides that have sufficiently long lifetimes to be produced at another accelerator are given in blue.

Measurements of nuclear reactions that provide the essential information are often difficult to carry out with the low intensity of the short-lived beams. Direct reactions are

important because of their selective nature, and the relative simplicity of understanding the experimental observables. Single-nucleon transfer reactions, in particular, such as (d,p), (α,t) or (^{3}He,d) probe the basic single-particle structure of nuclei. Such studies have been important in the past for establishing the basic framework for the understanding of stable nuclei and are again coming to the fore in exploring this structure in nuclei away from stability, with the short-lived beams that are becoming available at accelerators in the US such as ATLAS, HRIBF, MSU and Texas A&M. These are but first exploratory steps for the most accessible of short-lived nuclei; the exploration of single-particle structure away from stability will be an essential early step in expanding the description and understanding of the much more exotic nuclei with the Rare Isotope Accelerator (RIA).

Such reactions with rare isotopes have to be studied with beams of the isotopes on light targets, in inverse kinematics for which the proposed solenoid has considerable advantages. The reactions of interest include:

- **Single-particle structure:** mapping out the single-particle strength near closed shells.
- **Astrophysics:** Reactions such as (d,p) or (^{3}He,d) can provide important information for the *s*, *r*, and the *rp* processes.
- **Pair transfer:** Reactions such as (p,t) and (t,p) and (^{3}He,p) probe the nature of pair correlations in a new domain away from stability.
- **Inelastic scattering** of protons, α and other particles, has the potential to probe more collective aspects of nuclear structure *(G. Kraus et al. Phys. Rev. Lett.* **73** *1773, 1994)* including ones not readily accessible by electromagnetic transitions.
- **Knockout reactions,** such as (p,2p) provide valuable information on the occupation of single-particle orbitals, particularly at higher energies. A solenoid may be useful below energies of ≈100 MeV/u.
- **Surrogate reactions,** which provide information related to cross sections in neutron-induced reactions on shortlived isotopes, and are needed for stockpile stewardship.

Some of these difficult measurements are now carried out with large and complex detector arrays. Many features of the proposed solenoid will help reduce the complexity and alleviate

some of the experimental difficulties. In the next 10 years before RIA, such a solenoid has a number of applications. Once developed and refined, the technique will impact the much expanded scope for reaction studies with short-lived beams at RIA.

A. Nucleon transfer reactions

Nucleon transfer is an essential probe of the single-particle component of the nuclear wave function. The success of microscopic *ab initio* calculations in reproducing the structure of light nuclei has stimulated considerable interest in testing them through the measurements of spectroscopic factors. A recent example is the ^{8}Li$(d,p)^{9}$Li reaction studied at ATLAS, through the $d(^{8}$Li,$p)^{9}$Li reaction *(A. H. Wuosmaa et al. submitted for publication, 2004)*. This reaction proceeds both to the bound states and the unbound resonances in the ^{9}Li system. The spectrum of protons and the angular distribution obtained are shown in Fig. 2. Such studies would be greatly facilitated with the new solenoid, resulting in data of improved quality in energy resolution, cleanliness, and requiring less beam time. As the ability to produce such beams increases at ATLAS and elsewhere, these exploratory measurements will provide a crucial testing ground for our understanding of nuclear structure.

Measurements with heavier nuclei have been carried out at ATLAS (e.g. ^{56}Ni$(d,p)^{57}$Ni and ^{56}Ni(^{3}He,$d)^{57}$Cu) *(K.E. Rehm et al. Phys. Rev. Lett.* **80** *676, 1998)* and at HRIBF (e.g. ^{78}Ge$(d,p)^{79}$Ge and ^{84}Se$(d,p)^{85}$Se) *(K.L. Jones et al. "Nuclei at the Limits", Book of Abstracts, 2004)*. Some of the results are illustrated in Fig. 3. These are some of the first attempts to explore single-particle structure on closed-shell nuclei that are not stable. Similar studies are planned with ^{132}Sn beams at HRIBF at sub-Coulomb energies, and at somewhat higher energies at ATLAS when the californium upgrade is completed. Such measurements are crucial for defining the framework for further studies of these nuclei. There are indications of changing single-particle energies as a function of neutron excess in stable nuclei *(J.P. Schiffer et al. Phys. Rev. Lett.* **92** *162501, 2004)* and evidence for changing magic numbers from studies of 2^{+} energies and B(E2) values, but transfer reactions on short-lived nuclei are needed to clearly identify the changing single-particle structure that must be responsible for this phenomenon.

Further away from closed shells such reactions are also a valuable tool to map out the deformation-driving single-particle orbits in nuclei further from stability. For instance, in

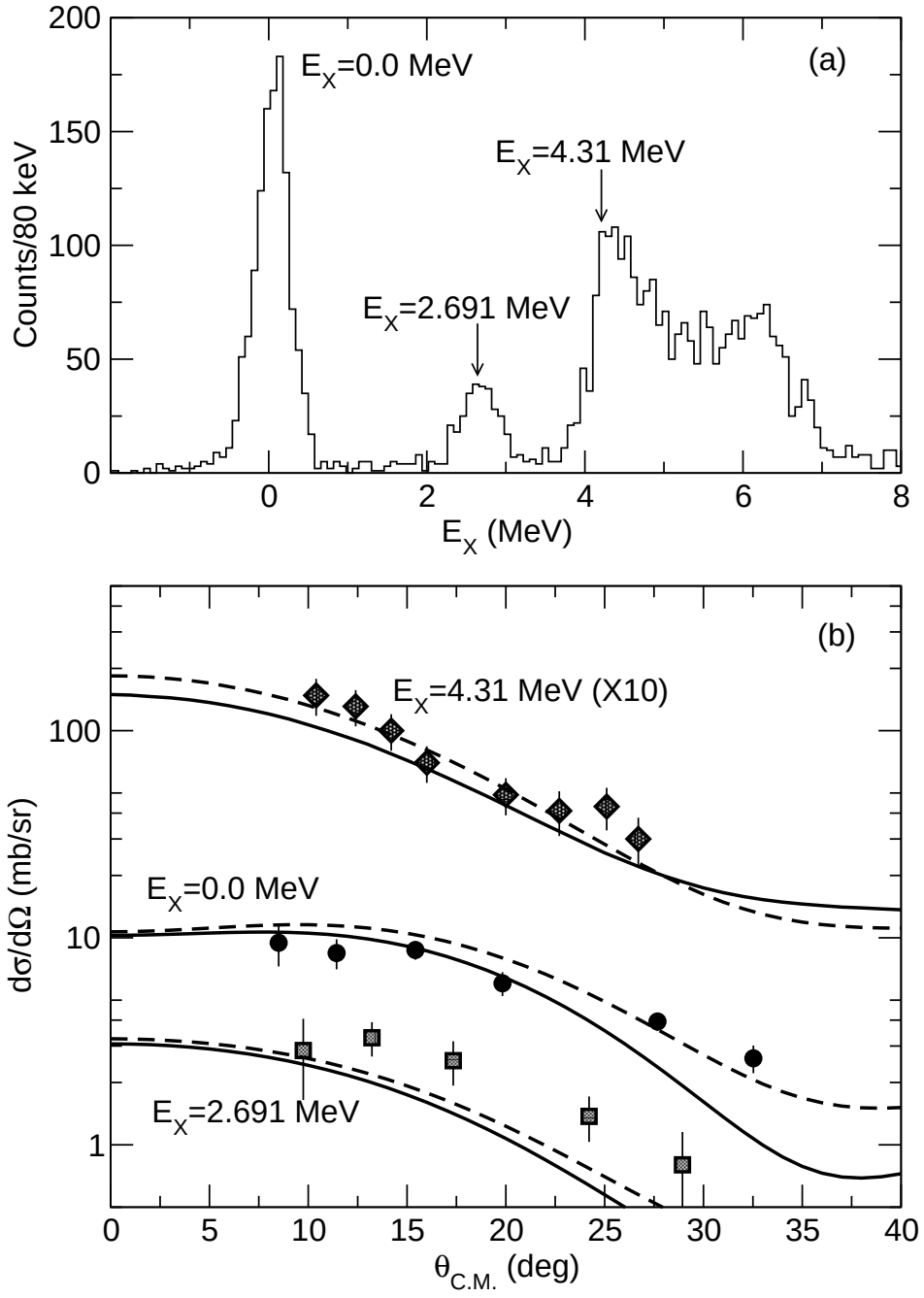

FIG. 2: (a) Excitation energy spectrum for the $d(^8\mathrm{Li},p)^9\mathrm{Li}$ reaction. (b) Proton angular distributions for levels in ^{9}Li.

approaching the N=Z region in the A=80 region there is evidence of oblate-prolate deformation, but the evidence as to its origins is indirect. Transfer reactions are needed to get the fingerprints of the Nilsson configurations to put this information on a firmer basis.

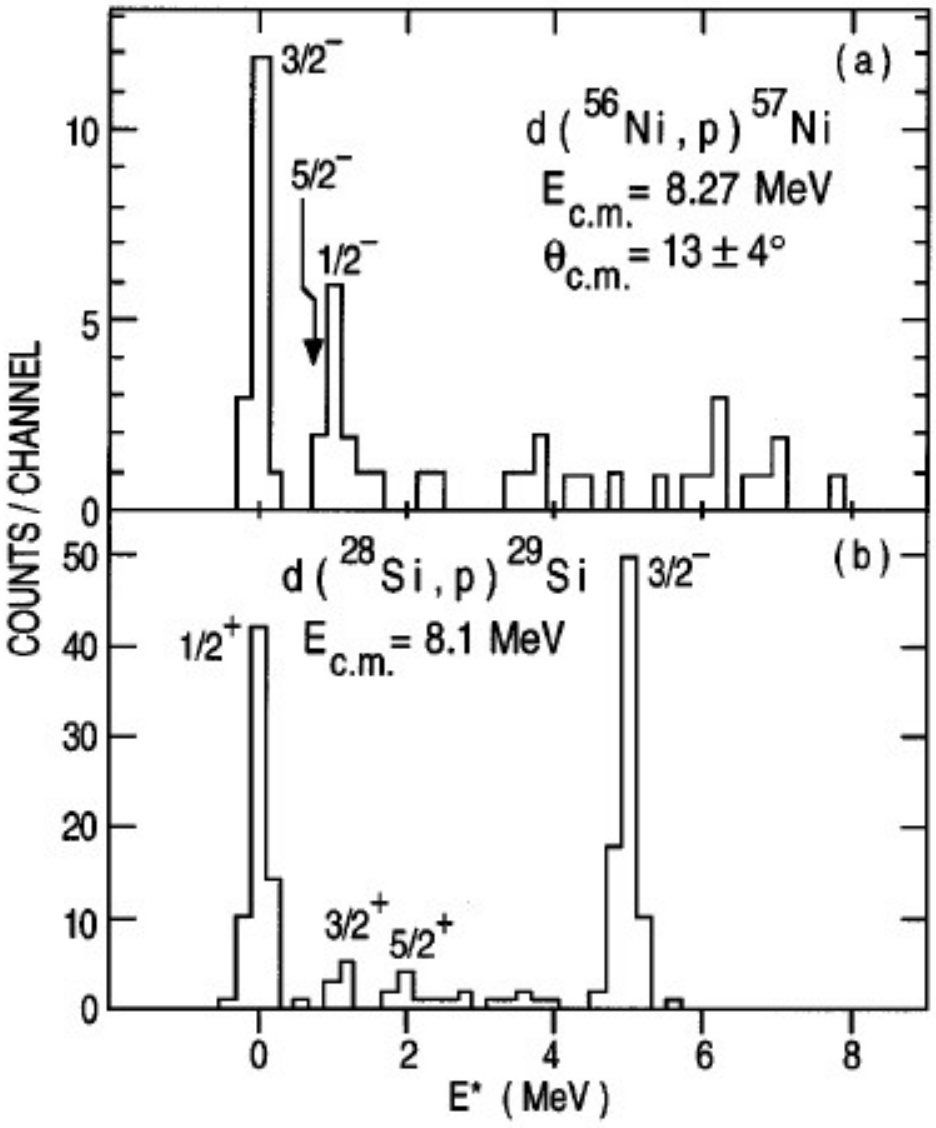

FIG. 3: (a) Excitation energy spectrum for the $d(^{56}\mathrm{Ni},p)^{57}\mathrm{Ni}$ reaction with a spectrum taken in the same detector array using a stable ^{28}Si beam for comparison.

B. Pair transfer reactions

The nature and strength of pairing correlations is an important aspect of nuclear structure. An example that would benefit from a solenoid spectrometer is the study of T=0 pairing in N=Z nuclei, particularly through $n-p$ pair transfer using (^{3}He,p) reactions in inverse kinematics with ^{44}Ti and ^{56}Ni beams at ATLAS. This form of pairing is expected in analogy with (a) the pairing between neutrons or protons coupling to T=1, 0^+ pairs that are strongly correlated and (b) with electrons in BCS superconductivity. It has been the sub-

ject of considerable speculation whether similar pairing might exist between neutron-proton pairs which can form deuteron-like T=0, 1^+ pairs as bosons. So far the experimental information is ambiguous. These effects are likely to be most pronounced in the heavier N=Z nuclei where both protons and neutrons are filling the same orbits near the Fermi surface. Pair transfer on ^{44}Ti and ^{56}Ni can be pursued further with beams presently available at ATLAS with an efficient detector. The improvement in resolution expected from a solenoid is evident in a simulation shown in Fig. 4. The center-of-mass energy resolution with the solenoid would be limited only by the resolution of the silicon detector, 50 keV FWHM, as shown in the lower part of the figure. In contrast, the resolution would be about 180 keV in a conventional array assuming the same detector resolution and a laboratory angle segmentation of 2°, as shown in Fig. 4(a). *(See A. Macchiavelli, Appendix B2 for more details).*

C. Astrophysics

Although a large fraction of nuclei in the universe is produced in the stellar cauldrons via radiative capture processes e.g. (n,γ) and (p,γ), light-ion induced transfer reactions, such as (d,p), (^{3}He,d), can provide crucial information for a better understanding of the astrophysical reaction paths. Some examples are given below.

In the r-process (i.e. the rapid addition of neutrons to medium mass seed-nuclei in a hot, neutron-rich stellar environment) nuclei located along a closed neutron shell (e.g. N=50, 82 and 126) act as so-called waiting points, where the reaction flow has to wait for the relatively slow beta decay, because the addition of a neutron is hindered by the very small neutron binding energy. A direct measurement of (n,γ) reactions on neutron-rich nuclei is impossible because of the short half-lives of these nuclei and the lack of a suitable neutron target. The only alternative is to use the correlations between (n,γ) and (d,p) reactions to obtain cross section information for nuclei along the closed neutron shells. Since the beam intensities for these nuclei away from stability are usually very small, a high efficiency, high resolution spectrometer is needed. Standard magnetic spectrometers have solid angles of 100 msr which is still a factor of 50 smaller than the proposed solenoid design.

Proton capture reactions (e.g. ^{25}Al$(p,\gamma)^{26}$Si, ^{29}P$(p,\gamma)^{30}$Si, ...) play an important role in the so-called rapid-proton capture (rp) process and are discussed in Appendix B3.

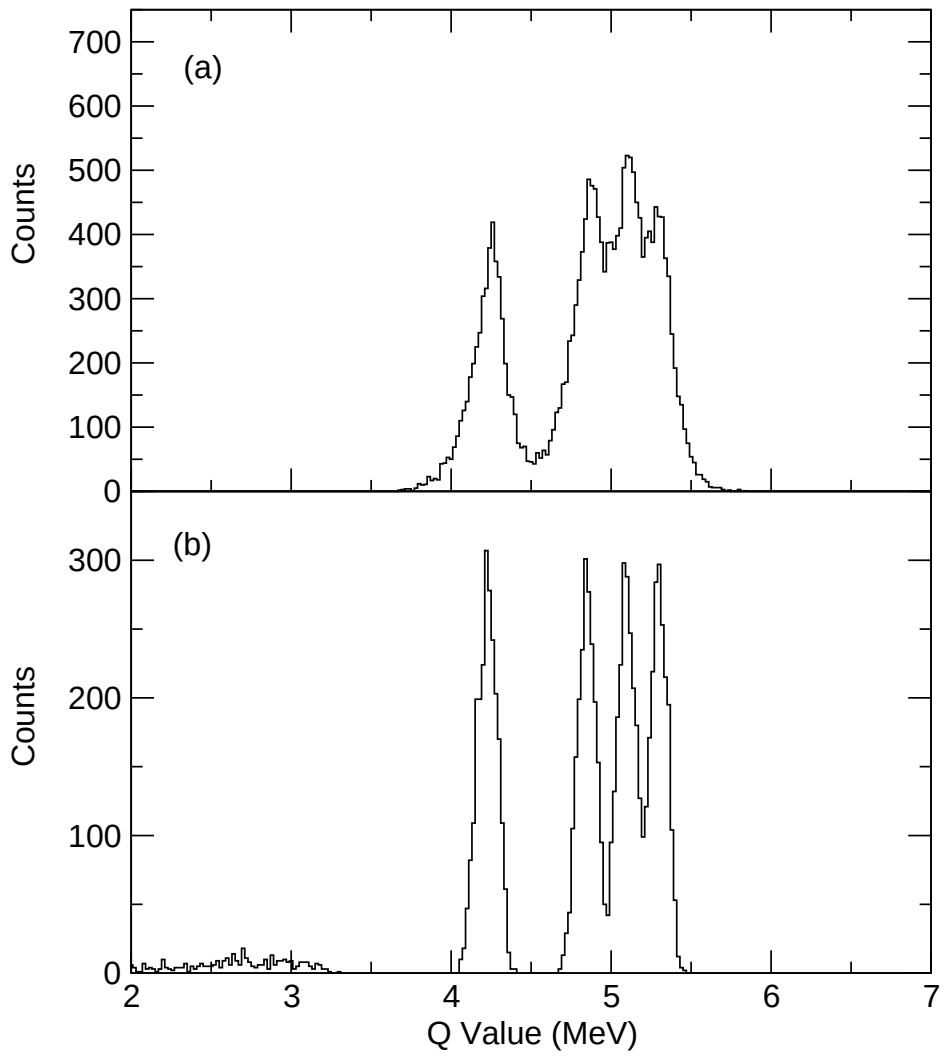

FIG. 4: Q-value spectra for the ^{3}He(^{56}Ni,p)^{58}Cu reaction reconstructed from (a) proton energy and angle with 2° resolution in a conventional array, and (b) proton energy and z in a solenoid with a position resolution of 1 mm and the same detector energy resolution. The details of this calculation are discussed further in the Sect. V on pages 36-38.

The isotope ^{26}Al ($T_{1/2}$=7×10^{5}y) has been found by several gamma-ray satellites, allowing the study of the history of explosive hydrogen burning in novae and supernovae covering the last 10 million years. Among the reactions which are important for producing ^{26}Al is the radiative proton capture reaction ^{25}Al$(p,\gamma)^{26}$Si going through several resonances in ^{26}Si. Despite many experiments utilizing e.g. (p,t), (^{3}He, n) and (^{3}He,^{6}He) reactions, the spin values of two unnatural parity states (1^{+}, 3^{+}) in ^{26}Si are still under debate. According to Ref.*(J. A. Caggiano et al., Phys. Rev. C* **65***, 055801, 2002)* the 1^{+} state at E_x=5.678 MeV

dominates the astrophysical reaction rate at temperatures below T_9=0.2, while at higher temperatures the 3^+ state at E_x=5.945 MeV and the neighboring 0^+ state at 5.916 MeV contribute about equally to the rate. The 3^+ and 1^+ states are only weakly populated in two-particle transfer reactions, but should dominate the angular distributions of ^{25}Al(^{3}He, d)^{26}Si at forward and intermediate angles because of the $5/2^+$ spin of the ground state of ^{25}Al. This is an experiment that could be performed with a 150 MeV ^{25}Al beam from the in-flight facility at ATLAS utilizing the compact ^{3}He gas target. It should be noted that the spin-assignment and the excitation energies are still subject to discussions. A new, independent experiment would be an important step toward a better understanding of ^{26}Al production in our galaxy. Similar (^{3}He, d) studies could be performed with other beams (e.g. ^{29,30}P and ^{31}S) available at existing radioactive beam facilities.

Although direct cross section measurements with radioactive beams have been performed for some cases (e.g. with a ^{21}Na beam), indirect methods will be the main techniques until beams with sufficient intensities become available at RIA. In the indirect techniques, information about the critical widths Γ_γ and Γ_p are obtained from either half-live measurements using GAMMASPHERE *(D.G. Jenkins et al. Phys. Rev. Lett.* **92** *031101, 2004)* or from spectroscopic factor measurements (e.g. via the (^{3}He,d) reaction with a radioactive beam) *(K.E. Rehm et al. Phys. Rev. Lett.* **80** *676, 1998)* populating states above the proton threshold in the final nucleus. This requires a compact gas cell target which has been in operation at ATLAS for the last five years. The superior Q-value resolution obtainable with the solenoid will make this device an excellent tool for a study of the rp-process involving heavier nuclei.

For the reaction flow in the *rp* process, high precision mass values of drip line nuclei are needed. While this is possible with present techniques for isotopes with half lives down to the one second range, masses of nuclei beyond the drip line are not accessible with this technique. These (particle-unstable) nuclei can play a role for processes involving the successive capture of two protons through a slightly unbound intermediate nucleus. An example is the waiting point nucleus ^{68}Se which can be bypassed via the ^{68}Se($2p, \gamma$) reaction.

D. Inelastic scattering

Inelastic scattering of protons, alpha particles, etc. can help access more collective modes, and can be particularly useful in cases where Coulomb excitation is not practical. The region of interest is always in the vicinity where the momentum transfers are relatively small. This means that the recoil particles to be detected have relatively low energies, and are scattered slightly forward of 90^o - suitable for detection in a solenoid. Such studies would be of interest at ATLAS when the energy upgrade now under way is completed as well as at MSU and at Texas A&M. An example is the ^{56}Ni(p,p') study that was carried out at GSI at higher energies *(G. Kraus et al. Phys. Rev. Lett.* **73** *1773, 1994)*. Since the same momentum transfers, and thus the same recoil proton energies, are of interest to extract collective matrix elements, a solenoid would be an equally useful spectrometer regardless of the bombarding energy. For example, the matrix element for exciting the 1.08-MeV first-excited 2^+ state, and possibly those for higher states, in ^{44}Ti could be investigated at 15 MeV/u with a beam that could be produced at ATLAS after completion of the current energy upgrade.

Another interesting possibility is the study of proton knockout (*e.g.* $(p,2p)$ reactions), which can be done at energies available at MSU up to 100 MeV/u. Here the solenoid would be an ideal device, allowing a large solid angle for the detection of both protons, although detectors would have to be thick enough to stop the protons. These studies may require a reconfiguration of the target and detector position to allow for longitudinal flight paths longer than the nominal 75 cm in order to extend the proton acceptance to higher energies.

E. Stockpile stewardship

The stockpile stewardship program relies on accurate physics data that are used in simulations. Many of these are neutron cross sections on nuclei that are not stable. Since they are not accessible to direct measurements, indirect 'surrogate' techniques, such as (d,p) reactions are needed. The example of the ^{95}Sr$(d,p)^{96}$Sr reaction is discussed by *K.L Jones and L. Ahle* in Appendix B1.

F. Summary of scientific justification

In this section we have emphasized the scientific importance of obtaining nuclear structure information for exotic nuclei by studying transfer and other light-ion reactions. The new device opens the way for an efficient way to carry out such studies at the new frontier of unstable nuclei employing inverse kinematics with unstable beams, at existing facilities (e.g. ATLAS, HRIBF, MSU and Texas A&M) and leading to RIA. In the following section we will show that the proposed solenoid spectrometer is an almost ideal device, combining an optimization of the solid angle coverage with a circumvention of the inherent loss of dispersion in inverse-kinematic studies.

III. CONCEPTUAL OVERVIEW

A. Introduction

Most short-lived nuclei are produced in such small quantities that, in order to study reactions, they have to be used as beams rather than targets. It is, therefore, necessary to employ inverse reactions, in which very light targets are bombarded with energetic beams of the heavier short-lived nuclei. Inverse reactions present significant challenges to experimental investigation.

At energies above the Coulomb barrier the relevant information is in the forward peak of the angular distribution in the center of mass. In the inverse process, the light reaction products are therefore often emitted with small energies in the laboratory, and the Jacobian transformation from center-of-mass frame to laboratory frame is highly unfavorable so that the particles emitted in a small range of center-of-mass angles are distributed over a larger region of laboratory angles. In such cases the energy scale of the light particles in the center-of-mass frame will be compressed, and, thus, the energy resolution in the center-of-mass frame will be significantly worse than that in the laboratory by as much as a factor between 3 and 10. In other cases, the kinematics force the forward center-of-mass particles to be compressed into a small angular range near 90 degrees in the laboratory, with the particle energy changing rapidly in a small angular interval. This again has a severe impact on the resolution that can be obtained. Resolving peaks corresponding to closely spaced levels and obtaining the necessary information at forward center-of-mass angles thus requires:

- large acceptance and solid angle,
- good position (angle) resolution,
- excellent energy resolution
- good particle identification.

The need for large geometric acceptance is very important with unstable beams that are produced with low intensities. Conventional detector arrays that are used in this regime are large, multi-segmented, and complex. To optimize the energy resolution from Si detectors, cooling is usually necessary. This becomes awkward with large arrays. The identification

of low-energy charged particles requires either two layers of silicon detector in a ΔE-E arrangement, increasing the complexity of the array, or detectors that can provide sub-nanosecond time resolution to precisely measure particle time of flight. Both options are problematic, especially in the critical angle regions where the particle energies are low. In addition, large solid-angle silicon arrays can be sensitive to backgrounds including direct scattering of the beam, or beta particles /delta electrons that can be emitted in large numbers from the target.

As an example, we consider the case of single-nucleon transfer reactions on nuclei with mass A≈100, though the kinematics are similar over a wide mass range.

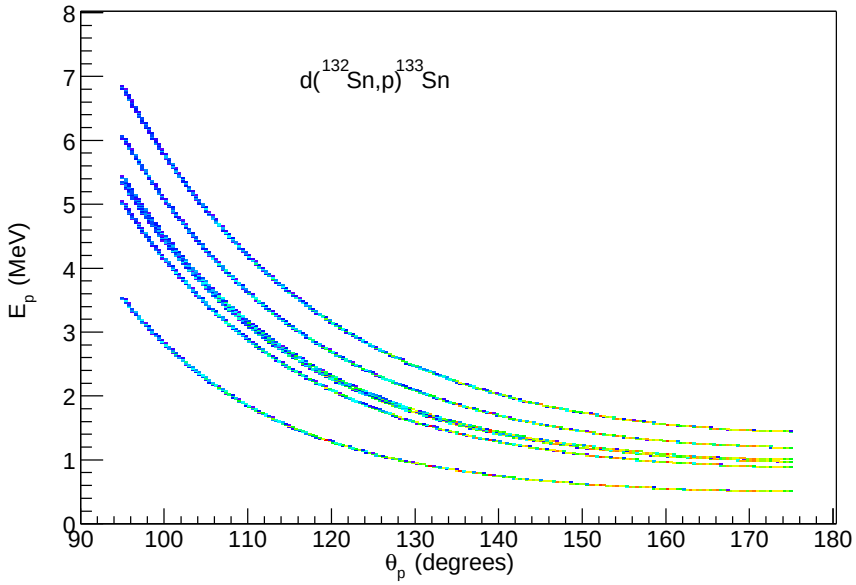

FIG. 5: Proton laboratory energy vs angle systematics, for $d(^{132}\mathrm{Sn},p)^{133}\mathrm{Sn}$ at 8 MeV/nucleon.

One case of interest now, and that is kinematically typical of many other reactions that are currently feasible at ATLAS, is the $d(^{132}\mathrm{Sn},p)^{133}\mathrm{Sn}$ neutron-transfer reaction, which probes the neutron single-particle levels outside the doubly-magic neutron-rich ^{132}Sn core. At sub-Coulomb energies, such a reaction cannot readily populate states with high orbital angular-momentum transfers, and the spectroscopic factors are very sensitive to the bound-state parameters. Ideally, this reaction would be done between 7 and 10 MeV/nucleon. The critical angular region in which the protons are to be detected is forward in the center of mass frame, corresponding to the backward hemisphere in the laboratory. Figure 5 shows the dependence of proton energy on laboratory angle for this reaction, for several states

in ^{133}Sn. At the angles of interest, these proton energies are typically 1-5 MeV, and are relatively insensitive to the bombarding energy.

As can be seen in Fig. 5, at backward angles in the laboratory the energy scale is "compressed" with a 1 MeV difference in excitation energy becoming a 0.2-0.3 MeV difference in the laboratory energies of the corresponding protons, thus compounding the energy resolution limitation of the detectors. A spectrum that would be obtained in a detector subtending an angle range of 2^o centered at 170^o in the laboratory appears in Fig. 6(a), whereas a spectrum obtained at a specific location on the solenoid axis is shown in Fig. 6(b). Note that the energy separation between individual states in the center-of-mass system is retained in the latter case, which allows for a better identification of individual states given a finite detector resolution. This is a major advantage of the solenoid system, which is discussed in more detail in Sects. V and Appendix A. Because of the center-of-mass to laboratory transforma-

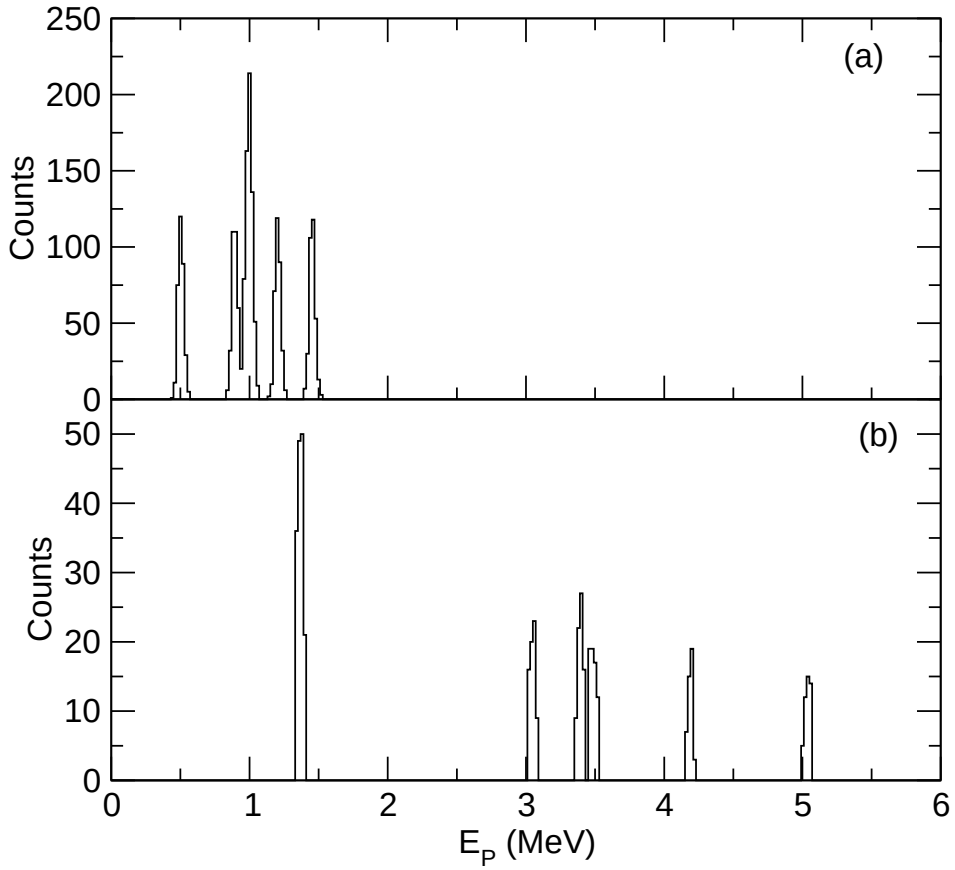

FIG. 6: (a) Proton energy spectrum at 169^o $< \theta_{lab} <$ 171^o for the $d(^{132}\mathrm{Sn},p)^{133}\mathrm{Sn}$ reaction at 8 MeV/nucleon. (b) Proton energy spectrum corresponding to a fixed position z ($\pm$1mm) on the solenoid axis.

tion, a large range of backward laboratory angles corresponds to a relatively small range of center-of-mass angles. It is therefore important to cover as large a solid angle as possible in order to optimize acceptance for the physically interesting angle range.

Other reactions pose similar problems. Transfer reactions such as (α, t), proton, or alpha particle inelastic scattering lead to particles emitted in the forward hemisphere, often with very large kinematic shifts ($dE_{lab}/d\theta_{lab}$). In such cases, the particles corresponding to two different center-of-mass angles will translate to the *same* laboratory angle making such studies particularly difficult.

The neutron transfer reaction ^{132}Sn$(d,p)^{133}$Sn has been used above as an example to outline the advantages of the new solenoidal spectrometer. While this reaction shows kinematics typical of many others, and the physics of this experiment (neutron transfer reactions along the N=82 closed-neutron shell) is very interesting, beams of ^{132}Sn at sufficiently high energies are still a few years away. To illustrate some different kinematics, we also discuss an experiment with an ^{25}Al beam available at ATLAS (see also Sect. II). The ^{25}Al(^{3}He,d)^{26}Si reaction would be studied at forward and intermediate angles at a bombarding energy of 6 MeV/u. The kinematics for populating the critical states at a bombarding energy of 6 MeV/u is discussed in Sect. V and a simulation of the achievable Q-value resolution of ∼130 keV is shown in Fig. 7. While the resolution of the solenoidal spectrometer should be sufficient to separate the 1^+ state at E$_x$=5.678 MeV from the neighboring 4^+ state at E$_x$=5.518 MeV, the small separation (ΔE= 29 keV) between the 0^+ and 3^+ state at E$_x$=5.916 and 5.945 MeV, respectively will allow only to extract a combined cross sections from the angular distribution.

B. The Solenoid Spectrometer

Many of the difficulties experienced with large Si-detector arrays can be overcome with a technique that utilizes a large-bore, uniform-field magnetic solenoid with $\mathcal{B}$ ≈2 to 5 Tesla as a particle spectrometer. In this method, illustrated in Fig. 8, the heavy-ion beam is aligned with the magnetic axis of the solenoid. The beam bombards a target inside the field, consisting of either a foil or a windowed gas cell. Particles emitted from the target follow helical cyclotron trajectories in the magnetic field, and after a single orbit return to the solenoid axis. Some aspects of particle transport in a solenoidal spectrometer are

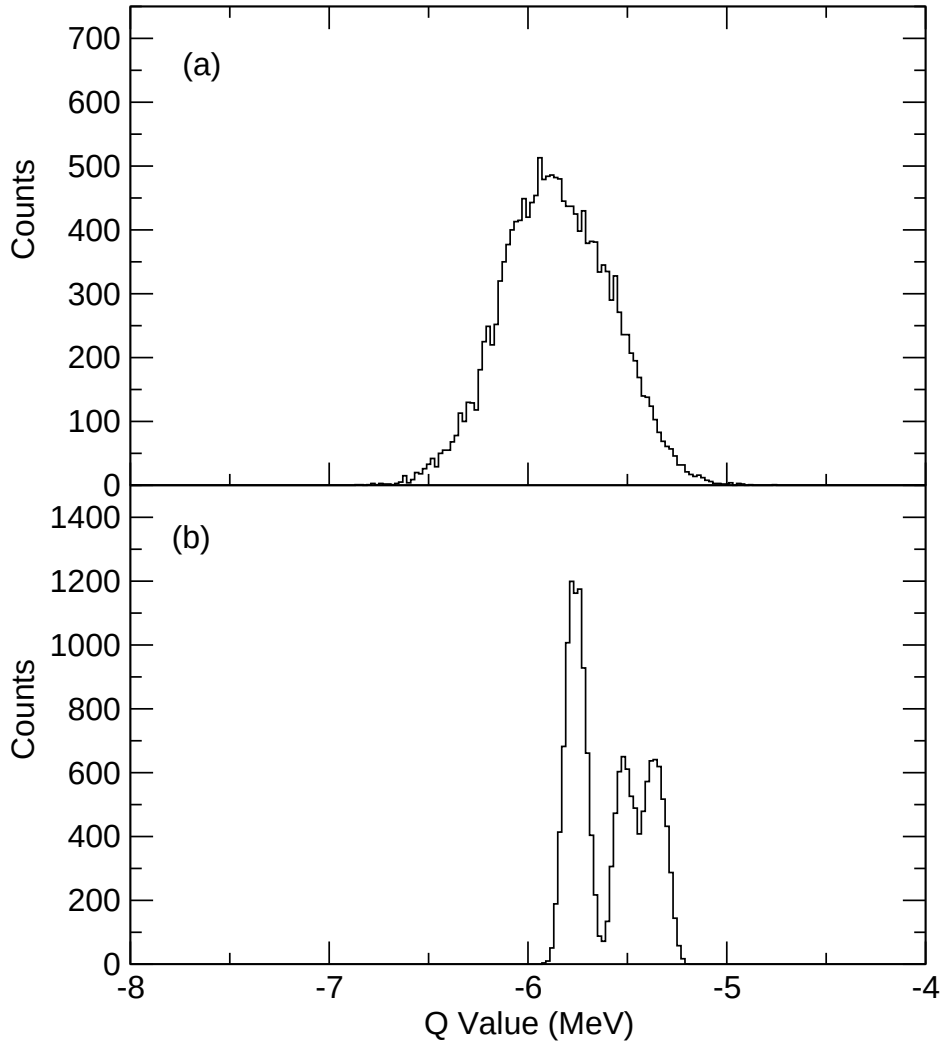

FIG. 7: Q-value spectra for the ^{3}He(^{25}Al,d)^{26}Si reaction reconstructed from (a) deuteron energy and angle with 2° resolution in a conventional array, and (b) deuteron energy and z in a solenoid with a position resolution of 1 mm and the same detector energy resolution. The details of this calculation are discussed further in the Sect. V on pages 37-39.

discussed in Appendix A.

The particles are detected using a hollow, pencil-shaped array of silicon detectors that is also placed on the solenoid axis as illustrated in Fig. 8. The detectors are position sensitive in the longitudinal direction. The silicon detectors measure the particle's energy, distance from the target, and flight time. An important difference between this scheme and the conventional detector array is that the particles are *not* detected at a fixed laboratory angle, but rather at a fixed *distance* from the target. The particles travel a fixed period of time

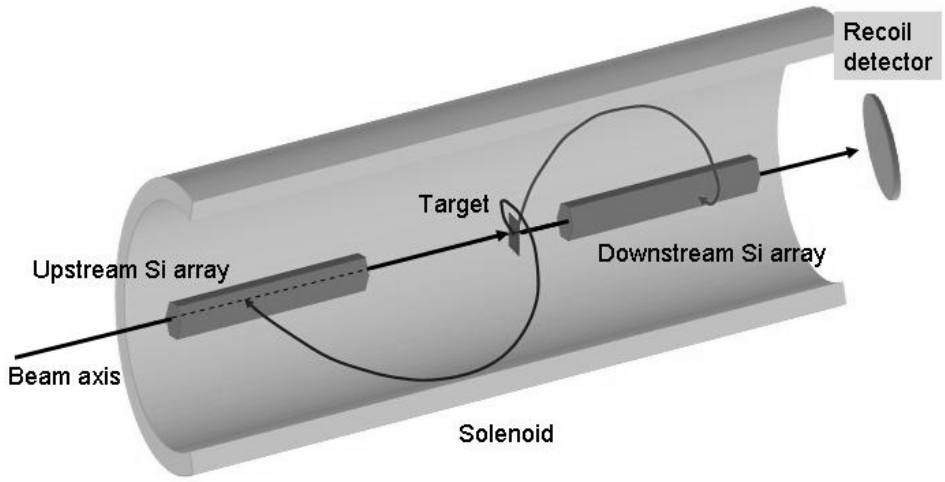

FIG. 8: Schematic illustration of a solenoidal charged-particle spectrometer.

$t = T_{cyc}$, where T_{cyc} is the cyclotron period given by

$$T_{cyc} = \frac{2\pi m}{qe\mathcal{B}}. \tag{1}$$

Here m, q and $\mathcal{B}$ are the mass and charge state of the detected particle, and the strength of the magnetic field, respectively. In ns, the cyclotron period is

$$T_{cyc}(ns) = 65.6 \times \frac{A}{q\mathcal{B}}, \tag{2}$$

where A is the mass number. The cyclotron period is *independent* of all other factors such as energy or scattering angle, and can thus be used to identify particles with different values of A/q. Table I lists cyclotron periods for different light particles moving in a 2 and 5 Tesla magnetic field. These times differ by several tens of ns, and can be distinguished even with the rather modest timing resolution of one or two ns expected at the low energies of interest.

The particles of interest are dispersed according to their velocity parallel to the beam direction. This mode of separation can be used to detect particles emitted into either the forward or backward scattering hemispheres, with the detector placed downstream and/or upstream of the target, and has several distinct advantages over more conventional methods.

All particles that do not impact the inner wall of the chamber inside the solenoid must eventually return to the solenoid axis, providing that they do not leave the magnetic field. Thus, all such particles can in principle be detected, and in a very straightforward way the device provides very large geometrical acceptance, subtending essentially all of the available

TABLE I: Cyclotron periods for various particles calculated with $\mathcal{B}$=2 and 5 Tesla.

Particle	T_{cyc} (ns) for 2T	T_{cyc} (ns) for 5T
p	32.8	13.1
d, α	65.6	26.2
t	98.4	39.4
^{3}He	49.2	19.7

2π azimuthal angle range. With two Si detector arrays, one before and one after the target, close to 4π solid angle can be attained, if necessary. The exact angle-energy acceptance of the transport device depends on the length and position of the silicon-detector array, the geometry of the solenoid, and the value of the magnetic field (see Appendix A).

The beam and the heavy recoiling partner are essentially unaffected by the magnetic field and exit the device. These ions may be detected in a subsequent set of downstream heavy-ion detectors with Z-identification. This method also provides a very simple method of particle identification. Since each detected particle executes a single cyclotron orbit, it's flight time is simply the cyclotron period, given by Eq. 1

An illustration of some typical trajectories for protons from the $d(^{132}\mathrm{Sn},p)^{133}\mathrm{Sn}_{g.s.}$ reaction at a bombarding energy of 8 MeV/u appears in Fig. 9. The distance from the solenoid axis versus position along the axis for protons emitted at angles of 110°, 135°, and 160° is shown in panel a), whereas the same orbits projected onto the transverse plane are shown in panel b).

Another major advantage of the solenoid method is that the center-of-mass energy resolution that can be obtained. Particles with trajectories that intercept the axis at the same point will differ in their energies by the *same* amount as the excitation-energy difference in the center of mass. This separation is achieved because the laboratory energy of particles with a particular value of m/q detected at a given position z on the solenoid axis is related to the center-of-mass energy solely by additive constants that depend only on the beam energy and z (see Eq. A9 in Appendix A). This feature implies that the effective resolution with the solenoid can be considerably better than with a conventional array.

This effect is illustrated in Fig. 10 which shows the energy versus z_p relationship for

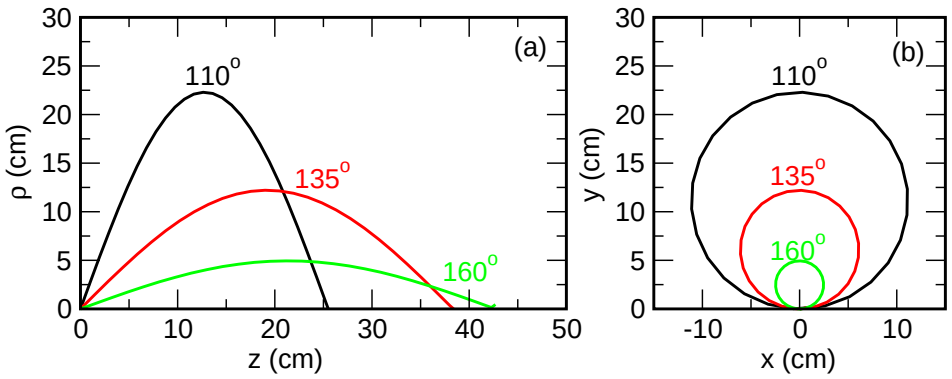

FIG. 9: Trajectories of protons from $d(^{132}\mathrm{Sn}, p)^{133}\mathrm{Sn}$ at 8 MeV/nucleon, for angles of 110°, 135° and 160°. (a) distance from solenoid axis versus position along axis. (b) view perpendicular to solenoid axis.

protons from the $d(^{132}\mathrm{Sn},p)^{133}\mathrm{Sn}$ reaction, for several low-lying states in $^{133}\mathrm{Sn}$. The straight lines in Fig. 10 represent the kinematic lines for the case of an ideal uniform-field solenoid with a line detector placed on the solenoid axis. The energy separation between different kinematic groups is clearly greater than that in the energy versus angle plane shown in Fig. 5. The corresponding energy spectrum that would be obtained at that position is then given by the indicated projection of that two-dimensional plot; the projected energy spectrum appears in Fig. 6(b). The peaks corresponding to different excited states are now separated by an energy difference equal to the separation in excitation energy, in contrast to the spectrum shown in Fig. 6(a).

The emission angle of the particle in the laboratory system may then be deduced from the position along the axis, combined with the energy of the detected particle. The physically important quantity, however, is the center-of-mass scattering angle. Once the particles are identified, and the Q value or excitation energy determined from the particle energy and position, the center of mass angle is given by

$$\cos\theta_{cm} = \frac{v_{lab}^2 - V_{cm}^2 - v_0^2}{2v_0 V_{cm}} \tag{3}$$

where V_{cm} is the velocity of the center of mass system (fixed by the beam energy), v_0 is the velocity of the particle in the center of mass system (fixed by the beam energy and Q value), and v_{lab} is the velocity of the particle in the laboratory, determined from the particle's energy.

Note that the surface area of Si detectors and the number of segments and channels of

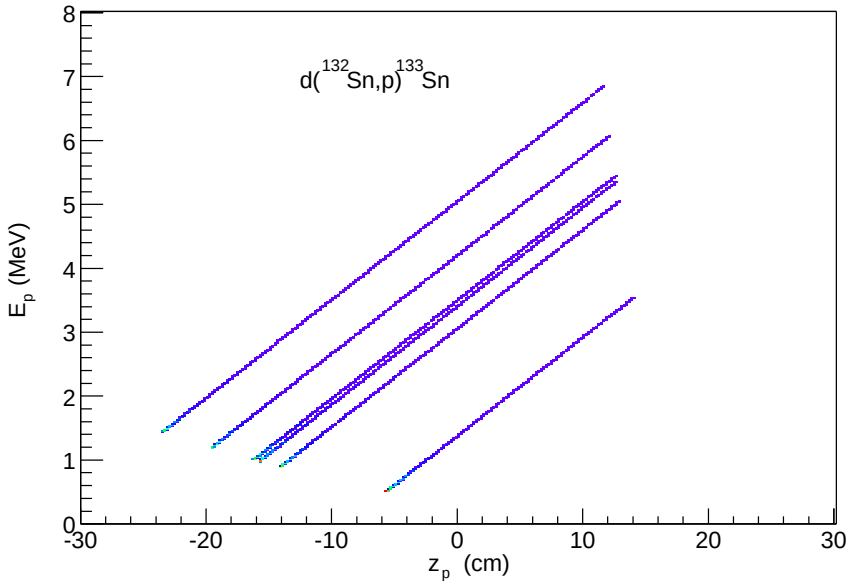

FIG. 10: Proton energies versus $z_{solenoid}$ for states in ^{133}Sn populated in $d(^{132}\mathrm{Sn},p)^{133}\mathrm{Sn}$ at 8 MeV/nucleon.

electronics will be significantly (perhaps an order of magnitude) lower in a solenoid compared to a large conventional detector array. This will also mean that cooling the detectors will be much simpler than cooling a large complex array.

Finally, this method also eliminates a large class of potential background processes due to the fact that only particles with the appropriate magnetic rigidity are transported from the target to the detector. Electrons, or beta particles are eliminated. Also, scattered beam particles have large velocities and, consequently, cannot be brought back to the axis where they would be detected.

In summary, using a large magnetic solenoid as a transport device for the study of reactions in very inverse kinematics offers substantial advantages compared to currently available alternatives:

- Large acceptance and solid angle
- Simple detector and electronics
- Straightforward particle identification
- Excellent center-of-mass energy resolution

- Excellent center-of-mass angle resolution
- Suppression of backgrounds

IV. TECHNICAL DESCRIPTION

A. Overview

In this section we describe the factors that lead to the design parameters for the magnet and silicon-detector array. The angle-energy acceptance of the device is determined by a combination of solenoid geometry, detector size and position, and magnetic field. In order to set the scale of the solenoid, one must consider the geometry and field strength needed to confine the most rigid light particles of interest, in particular tritons. In inverse kinematics, tritons emitted from a typical (α,t) reaction, with a large negative Q-value move forward in the laboratory. The most interesting region corresponds to the maximum angle, which can be between θ_{lab}=40° and 60°, depending on Q-value and beam energy. Here, the triton energy is generally between 5 and 10 MeV. The maximum distance ρ_{max} in meters that a particle travels from the solenoid axis is given by

$$\rho_{max}(m) = 0.290 \times \frac{\sqrt{EA}}{q\mathcal{B}} \sin\theta, \tag{4}$$

where E is the particle energy in MeV, A is the mass number, q is the charge state, $\mathcal{B}$ is the applied magnetic field in Tesla, and θ is the emission angle relative to the axis of the solenoid (and the beam axis). Similarly, the distance from the target to the point at which the particle returns to the axis is given by

$$z_0(m) = 0.911 \times \frac{\sqrt{EA}}{q\mathcal{B}} \cos\theta. \tag{5}$$

Figure 11 shows the values of ρ_{max} and z_0 as a function of emission angle relative to the solenoid axis for protons and tritons at various energies assuming a magnetic field of $\mathcal{B}$=5 Tesla. The dotted line in Fig. 11(a) and (b) corresponds to the acceptance limit imposed by a vacuum chamber with a 25 cm inner radius. The corresponding line in Fig. 11(c) and (d) shows the limit $z = 75$ cm such that particles return to the solenoid axis before leaving the device.

The shaded areas in Fig. 12 illustrate the overall device acceptance for (a) protons, and (b) tritons as a function of the particle energy and the angle of emission measured with respect to the solenoid axis. Here, the magnetic field is set at a value of $\mathcal{B}$=5 T, and the inner radius of the solenoid is 25 cm. The particles are accepted if their transverse distance from the axis is less than 25 cm, and if they return to the solenoid axis after traveling a

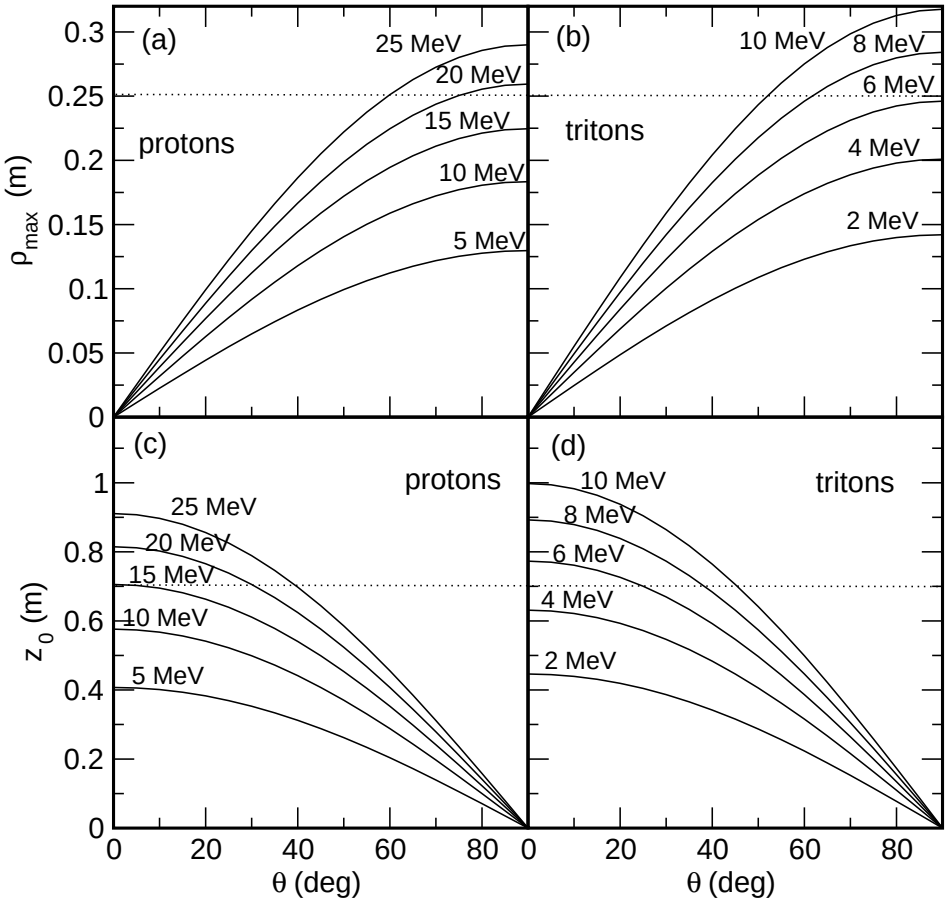

FIG. 11: (a), (b) Maximum perpendicular distance from the solenoid axis versus emission angle θ for (a) protons and (b) tritons with different energies. (c), (d) Distance z from the target at which (c) protons and (d) tritons return to the solenoid axis versus θ for different energies. The dotted lines indicate the limits on ρ_{max} or z imposed by a solenoid diameter of 0.5 m and maximum distance of 0.75 m from target to the end of the device.

distance of no more than 75 cm (one half of a 1.5 m long solenoid). The acceptance for a particular placement of the silicon detector and a specific magnetic field setting corresponds to smaller regions within the shaded areas of Fig. 12 as described in Appendix A.

B. Magnet

The required size (bore diameter and length) of the magnet for this system is determined by the acceptance calculations described above. Based on these simple considerations, the necessary solenoid dimensions are 0.5 m active diameter, and 1.5 m active length. With

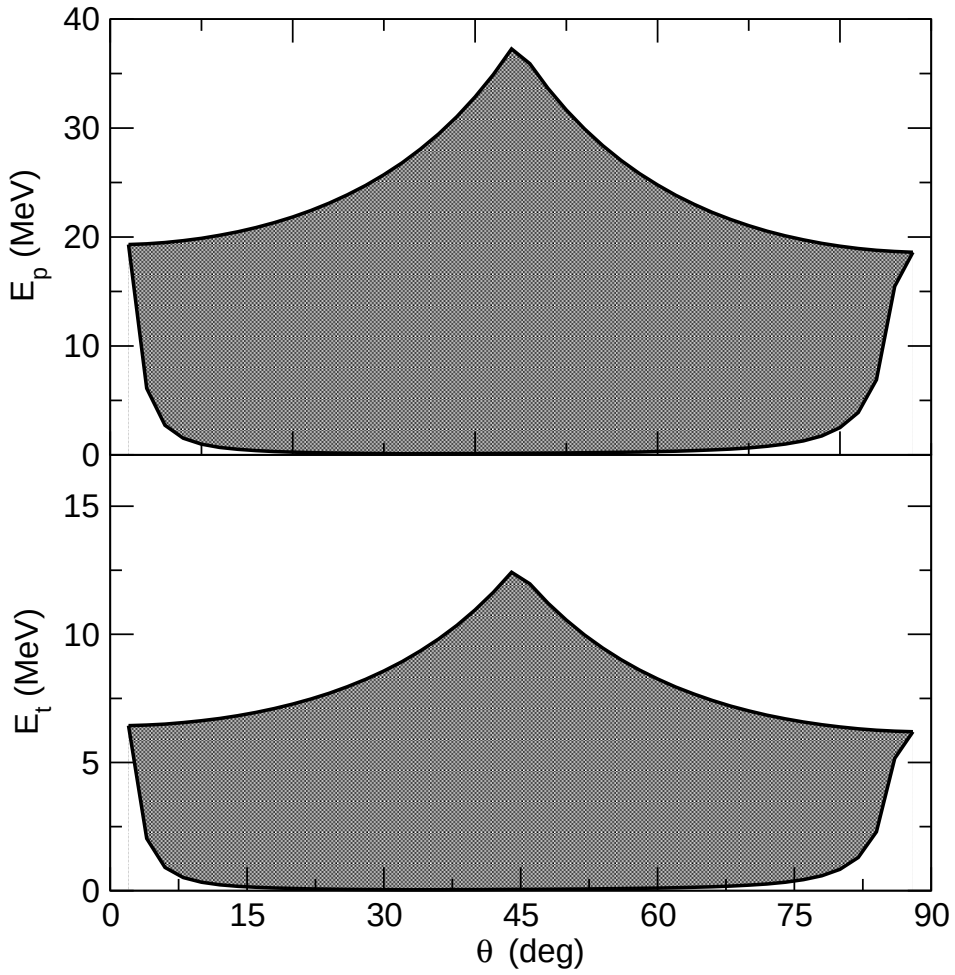

FIG. 12: Acceptance of the solenoid transport device for (a) protons (b) tritons. For $\theta \lesssim 43°$ the upper energy limit imposed by requiring particles to return to the solenoid axis within 75 cm from the target, whereas the energy is limited by the inner radius of the vacuum vessel (25 cm) at larger angles. The lower energy bounds are similarly set by the minimal orbits that will reach the detector surface, *i.e.* $\rho > 2$ cm and $z > 5$ cm.

this geometry, the maximum magnetic field must be no less than 5.0 Tesla. As discussed below, the uniformity of the magnetic field is an important consideration. Any cylindrical asymmetry in the field shall be less than 0.1%.

Magnets of this scale are not uncommon, and certainly not beyond the scope of current technology. Due to the high field and large bore, the solenoid must be a superconducting device. Such magnets are generally available from commercial manufacturers for use in, for example, magnetic-resonance-imaging (MRI) applications. The field uniformity for such

devices can be extremely high, of the order of 1 ppm for a spherical volume around the center of the solenoid and extending to the solenoid's inner wall, well beyond our current needs.

The magnet will be a so-called closed "cryogen-free" system, such that the cryogenic temperature will be maintained by one or more cryo-coolers, which are an integral part of the system. It will also be supplied with a superconducting "persistence switch", which can be used to isolate the device from the power supply once the magnet has been excited with the desired current, and it will be equipped with iron shielding to reduce stray magnetic fields.

C. Vacuum Vessel and Mechanical Components

The key mechanical support needs to be made of stainless steel or aluminum to avoid distortion of the magnetic field and be strong enough to support the solenoid that weighs $\sim$10 t without significant deflection. It must also have provisions for adjustments to allow precise alignment ($<$1 mm) of the solenoid on the beamline

Figure 13 shows a conceptual drawing that has been used to explore the mechanical implementation. The main vacuum chamber is a cylindrical vessel filling the bore of the solenoid that will allow uninterrupted orbits for the light particles in their trajectory between the target and the silicon array. It may be made of aluminum of $\sim$1 cm thickness, to avoid perturbation of the magnetic field. It could extend up to 10 cm beyond the magnet yoke, in order to be able to place the silicon array over the whole range of the magnetic field. The exact location of the vacuum vessel relative to the solenoid is not critical and can be centered on the bolt pattern of the solenoid faces. The whole solenoid and chamber can then be adjusted for height, position along the beamline, as well as for small angular adjustments.

All the critical components for the experiment will be mounted on the chamber end caps. The end caps will be mounted on rails that allow the arrays and targets to completely be removed from the solenoid for maintenance and target replacement. The frames that support, align and cool the silicon array are mounted on the end caps. The detector will be cooled by circulating an antifreeze/water mixture, which will allow the counters to operate down to -40 C°. The main cold finger will have some adjustment along the beamline ($\sim$10 cm) and will be made of modular sections to allow the front of the array to be mounted

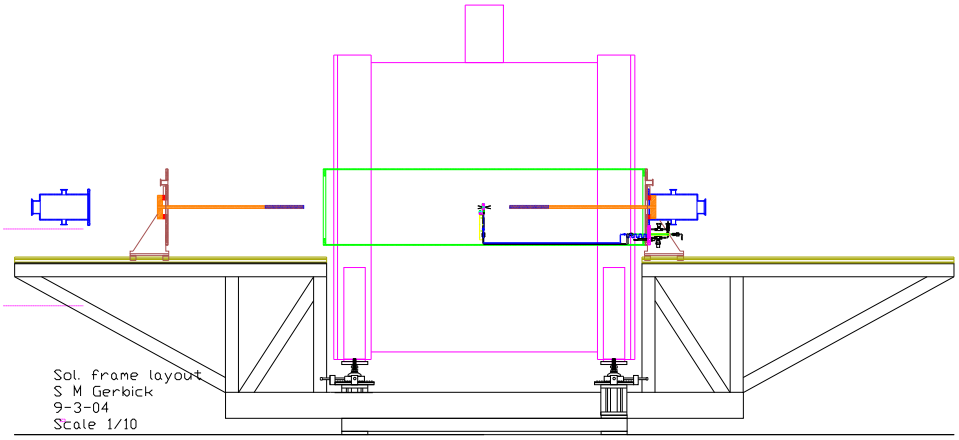

FIG. 13: Schematic technical drawing of the proposed solenoid spectrometer.

anywhere from 20 cm to 60 cm from the target location. The mounting will allow fine adjustment of the array to center it on the beamline and alter its "pointing" along the field. Attached to the outer face of the array will be a series of beam collimators and baffles that ensure the beam passes axially along the 1 cm diameter main array tube. Full alignment of all these components can be done using telescopes mounted upstream and downstream of the solenoid.

For a length of 3 m upstream and downstream of the array, the beamline will be free from components to allow the end caps to be fully removed. Lightweight beam pipes will span these gaps during operation and they will be removed to allow extraction of the end caps. At the outer end of these sections will be upstream and downstream pumping and diagnostic stations. Many components of pumping systems are susceptible to magnetic fields, leading to damage or malfunction, so remote stations seem advantageous. The stations will consist of oil free mechanical pumps to establish rough vacuum ($\sim$50μm) and then cryo pumps for establishing high vacuum. Extra pumping with pumping carts during primary installation and out gassing will be included. Full pressure diagnostics will allow pump-down at any speed (based on the fragility of the targets), but the fastest pump-down of back-filled dry gas will establish a high vacuum ($\sim 10^{-6}$ Torr) in $\sim$15 minutes.

D. Beamline

The north beamline in the general purpose area will be dismantled and completely reconfigured for the solenoid experiment. It will be repositioned at 20 degrees to the beam entry direction to maximize beamline length in the room. This line is nearly symmetric (20 degrees vs. 26 degrees) with the line going to the spectrograph and used for "in-flight" isotope production today. This line will be rebuilt with components similar to those of the spectrograph line, in order to facilitate tuning of radioactive beams from the production gas cells. In principle, new beams could be tuned and diagnosed using the spectrograph and its beamline, then the main magnet switched to the solenoid line for final focusing in the device.

E. Silicon Detector Array

The silicon-detector arrays, that detect the light charged particles, must provide a measurement of the particle's energy, distance from the target, and flight time. In addition, the detector array must be hollow so as to permit the beam to pass through to the target, and for heavy recoils to exit the system and be detected downstream. Another design requirement is that the upstream detector array, used primarily for studying (d, p), (^{3}He, p) and (^{3}He,d) reactions, should have as small a transverse dimension as possible, to avoid complications arising from small emission angles relative to the solenoid axis, and very shallow trajectories.

A conceptual design of the silicon detector array appears in Fig. 14. In this design, the detector arrays consist of 12 silicon detectors, each with dimensions 1 cm $\times$ 10 cm, made position sensitive along the long axis. The detectors are mounted to form a pencil-shaped array with a square cross section 1 cm on a side. In order to stop the most energetic protons of interest (up to 12 MeV), the thickness of the detectors is 1 mm. Such detectors are readily available and are well within the current capabilities of silicon detector fabrication technology.

The intrinsic energy resolution of each silicon detector element should be 50 keV (FWHM) for alpha particles. Due to the reduced straggling in dead layers for protons, the proton energy resolution will be slightly better. The timing resolution that can be achieved for such detectors should be sufficient to be able to distinguish particle species by their flight

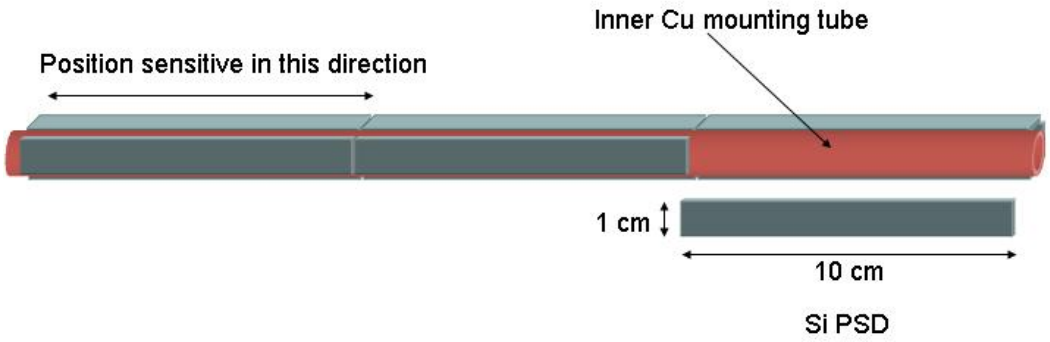

FIG. 14: Schematic design for silicon detector array.

times. As discussed above, a time resolution of better than 2 ns FWHM is more than sufficient for resolving the cyclotron periods associated with different particle species, and is readily achievable with currently available detectors and electronics. Simulations of the expected performance of the solenoid (see Sect. V) indicate that a position resolution of 1 mm, FWHM, is sufficient for distinguishing kinematic groups from states separated by as little as 100 keV in the center of mass frame. Since position-sensitive-detectors (PSDs) are available with intrinsic position resolution of 500 μm or better, this requirement is also readily satisfied using detectors similar to those commercially available.

The detector length is chosen to balance the particle acceptance (see above), which is in part determined by the length of the detector, and the desire to minimize the cost and complexity of the array. The 30 cm long detector provides good acceptance, with only 12 silicon sensors per array (see Appendix A). Depending on details of silicon sensor fabrication, the number of sensors could be increased to 16, and the length extended to increase the acceptance.

For particles emitted in the forward direction, the design constraints on the detector array are somewhat less stringent, as it is not as critical to detect particles that are emitted with small angles with respect to the beam direction. Here, the central hole in the array should be sufficient to accommodate the cone of recoil nuclei. For inverse kinematics in the mass A$\approx$100 region, this cone is very small, only on the order of 1^o or less. For lighter beams, however, the recoil cone can be as large as 7^o, and the hollow silicon detector must be large enough for these recoils to exit. A larger detector, of a roughly conical shape, would accomplish this task. In order to retain the efficiency, for a larger detector additional silicon detectors would be required to minimize gaps in the structure.

F. Electronics

Due to the relatively modest number of channels (~ 100) necessary for the instrumentation of the two silicon arrays, the electronics used to process the silicon-detector signals can use currently available off-the-shelf components. The requirements on the signal processing are that they provide energy resolution for 8 MeV alpha particles of 50 keV FWHM or better, that the position resolution achieved by resistive division be 1 mm or better (also essentially an energy resolution issue), and that the time resolution be of order 2 ns or better, FWHM. The only difficulty we forsee is the optimization of the timing measurement, which can be problematic for very low energy particles.

The position sensitive detectors possess three electrical contacts: one from the ohmic layer on the rear face of the detector and two from either end of the resistive division layer. Position sensitivity is obtained by comparing the signals from the two position contacts with the total energy signal from the rear, and readily yields position resolution values in the sub-mm range. The silicon-detector signal processing chain consists of a charge-sensitive preamplifier followed by shaping amplifiers and conventional analog-to-digital converters (ADCs). In order to process the timing information, a highly differentiated copy of the preamplifier signal from the back contact is discriminated, producing a logic signal that is compared with an external time reference, typically the RF pulse train from the accelerator. These timing signals are processed using conventional time-to-digital converters (TDCs). Detector bias voltages are applied using a commercially available multi-channel bias voltage supply system.

Similar systems are in common usage in many places, and the current application presents no significant challenges to existing technology. The silicon detector array system contains a total of 28 position-sensitive detectors and requires the instrumentation of 56 position channels, and 28 energy/time channels.

G. Target Mechanism

A good fraction of the experiments planned for the solenoid spectrometer requires the use of a gas target. Examples are (^{3}He, d), (^{3}He,α), (α, α'), (α, t) reactions. Since a windowless gas target is incompatible with applications requiring a large acceptance for the outgoing

particles, a localized gas cell target will be used. Such a target was developed at ANL and used for a variety of experiments with stable or unstable beams (e.g. ^{3}He(^{56}Ni,^{57}Cu)d, ^{4}He(^{44}Ti,^{44}Ti)^{4}He, and ^{3}He(^{20}Ne,^{19}Ne)^{4}He). The target consists of a 1 mm long cell filled with helium or hydrogen cooled to liquid nitrogen temperatures, in order to increase the total density. The entrance windows consist of 1.3 mg/cm^2 thick Ti foils which can sustain a pressure of 1 bar, resulting for helium in a target thickness of approximately 50 μg/cm^2. Reactions with the window foils can be eliminated by measuring the light particles in coincidence with the recoil particles (see Fig. **??** in Appendix B2). A modified version of this target will be used.

For experiments involving solid targets, a four sector, 2.5 cm radius, low-mass target wheel (similar to those used in GAMMASPHERE) will replace the gas cell. The drive will be using stepping motor and an absolute encoder to ensure reproducibility of positioning. Usually, the wheel will not rotate continuously but will be turned to move the target spot or to position a new target in the beam. However, the capability for continuous rotation will be available if target volatility is an issue.

Both the gas cell and solid target mechanism have their connections at the extreme periphery of the chamber to block as few trajectories as possible.

H. Recoil Detectors

1. $\Delta E - E$ array used for $A \leq 20$ recoils

For light-ion reactions with $A_{beam} \leq 20$, it is possible to detect and identify the recoiling beam-like particles using silicon detectors in a ΔE-E arrangement. Currently, silicon ΔE detectors are available in thicknesses as low as 30 μm, and readily available with thicknesses greater than 50 μm. In order to identify recoils with $A \leq$20, this corresponds to a threshold energy of between 2.5-3 MeV/nucleon for a 30μm thick ΔE, and 3.5 to 4.5 MeV/nucleon for a 50μm thick ΔE detector. A modest array of four ΔE-E telescopes that covers a large fraction of the 2π azimuthal angle range, such as that described in Ref. (*A. Wuosmaa et al, submitted to Phys, Rev. C*), could provide the recoil detection for reactions involving light exotic beams. In that case, the recoil detector with an inner active diameter of 1 cm and an outer diameter of 15 cm covers a range between approximately 1 and 7 degrees when placed

approximately 40 cm from the target. Such a detector could easily be installed within the solenoid volume, as the magnetic field has little effect on the performance of such detectors. Should scattering cause a rate problem in the silicon, an annulus with a larger diameter hole could be used, or the detector could be placed further from the target.

2. Gas ionization chamber used for $20 \leq A \leq 150$ *recoils*

In many cases with radioactive ion beams from, for example, accelerated fission fragments from the proposed Cf upgrade, the incident beams may not be isotopically pure. A recoil detector providing Z and A sensitivity is needed to identify the projectile-like recoils near 0°. For heavy ions, a suitable choice would be a gas-filled gridded ionization chamber to make measurements of the total energy and rate of energy loss. An isobutane-filled device could be made fairly compact; polypropylene windows with thicknesses of 2μm can contain gas pressures of up to 250 Torr, in which the range of *e.g.* ^{90}Sr ions at 15 MeV/A is around 30 cm. An anode segmented perpendicular to the zero-degree direction provides energy-loss measurements, which can be used to identify the atomic number of the ion. The total energy, reconstructed from the anode segments, may also be useful in specifying the kinematics of the reaction. The energy signal from each anode segment can usually be measured with a resolution down to around 1%. Gas is recycled and maintained at a constant pressure using a suitable baratron-controlled gas handling system.

Since the beam may be dumped into the detector itself, the design needs to accommodate as high a counting rate as possible. In order to reduce the rate in individual electronic channels, the anode can also be segmented along the zero-degree direction, as long as there is some divergence of ion trajectories spreading the ionization laterally. Space-charge effects will, however, eventually limit the operation of the device and some development is necessary to determine exactly how high this limit can be pushed, but it is expected that this limit will approach 100k ions per second. Such a limit should encompass most of the radioactive beams expected for ATLAS.

In order to provide a good timing signal for the recoil detector, a thin particle detector can be placed in front of the ion chamber, *e.g* a parallel-gridded avalanche counter. Time-of-flight measurements, coupled with the total-energy signal in the ion chamber, could be used to deduce mass information. Such thin particle detectors can be made position sensitive,

whilst still having high count-rate capability ($< 10^6$Hz, depending on size and readout arrangements), thus yielding information on the direction of the ion trajectory. This can be used both to place restrictions on the reaction kinematics as well as to optimize ion-chamber operation by path-length correction of energy-loss data.

The recoil detector will be placed at a position where the residual field from the solenoid does not affect its operation. This also has the advantage of increasing the time of flight for the recoils. In addition, such an arrangement will make best use of the angular dispersion of the recoils in spreading out ionization laterally in the gas detector, reducing rates in an individual electronic channel for an ionization chamber with lateral segmentation.

V. EXPECTED PERFORMANCE

A. Simulations

In order to realistically assess the resolution and transport properties of the solenoid spectrometer, we have undertaken a detailed study of the expected performance using Monte Carlo simulations that take into account detector size and misalignment, magnetic field non-uniformities, target thickness effects, and detector resolution effects. We consider the benchmark reactions that can be carried out using currently available ATLAS beams discussed in Sect. II with kinematics typical of a wide range of other reactions: ^{3}He(^{56}Ni,p)^{58}Cu, ^{3}He(^{25}Al,d)^{26}Si, and p(^{44}Ti,p')^{44}Ti. The bombarding energies used for these three reactions were assumed to be 5 MeV/nucleon, 6 MeV/nucleon, and 15 MeV/nucleon, respectively.

B. Base performance with ideal system

We begin by examining the transport performance in the case of an ideal, uniform magnetic field, and a cylindrical detector of radius 1 cm and length 30 cm placed on the solenoid axis. In each case, the emitted particles are tracked from their point of origin at the target to the silicon detector. Particles whose orbits are larger than the solenoid inner diameter, here assumed to be 0.5 m, will strike the chamber wall and thus are not detected. Particles that return to the axis at a position not covered by the detector will be blocked and are similarly lost. The applied magnetic field and the distance between target and detector are chosen in each case to optimize the detection efficiency for particles emitted at the angular range of interest. For ^{3}He(^{56}Ni,p)^{58}Cu, this corresponds to backward emitted protons. For deuterons from ^{3}He(^{25}Al,d)^{26}Si, the most important laboratory angles are slightly forward of 90°. In all cases, the energy resolution for the silicon detector is assumed to be 50 keV, the position resolution is 1 mm, and the time-of-flight resolution 1.5 ns, all FWHM.

1. The ^{3}He(^{56}Ni,p)^{58}Cu reaction

The kinematic curves of proton energy as a function of laboratory angle for the ^{3}He(^{56}Ni,p)^{58}Cu reaction are shown in Fig. 15, for states at excitation energies of 0.0, 0.203, 0.444, and 1.052 MeV. The large positive Q-value (Q=5.403 MeV) for this reaction results

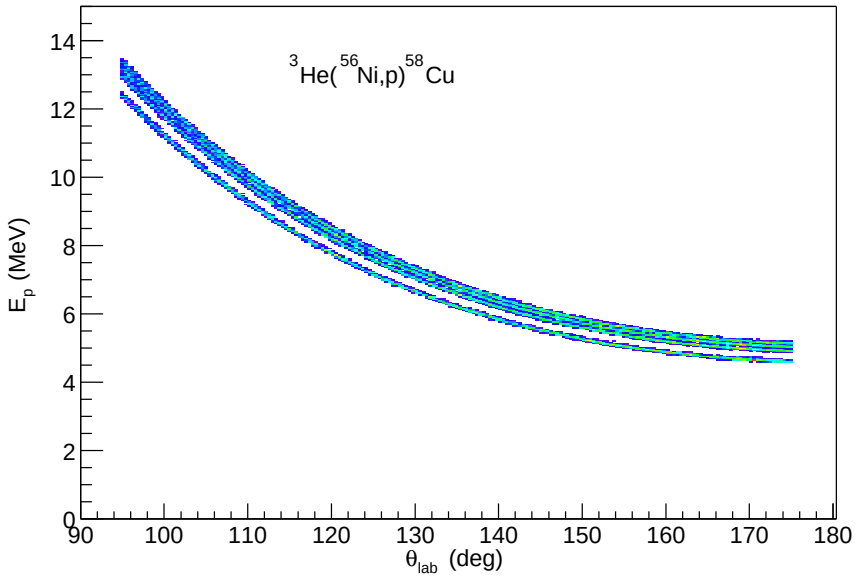

FIG. 15: Proton energy versus laboratory angle for various states in ^{58}Cu from the ^{3}He(^{56}Ni,p)^{58}Cu reaction.

in higher proton energies than for a typical (d, p) reaction in inverse kinematics (see Fig. 3 in Sect. II).

Figure 16 shows the dependence of the detected proton energy on the distance z for protons from ^{3}He(^{56}Ni,p)^{58}Cu. For this reaction, the magnetic field is 4.0 T, the target is placed 10 cm downstream from the center of the solenoid (z_{tgt}=10 cm), and the detector array covers from -42 cm to -12 cm. The different lines correspond to different excited states in ^{58}Cu. Over most of the region the lines are straight, in contrast to the kinematic dependence of proton energy on laboratory angle. At any fixed z the separation in proton energy between the different groups is equal to that between their excitation energies.

The deviation of the E_p vs z_p trajectories at the most backward angles arises because the particle trajectories are intercepted by the silicon detector array before returning to the beam axis. For very shallow angles of emission relative to the solenoid axis, the particles are detected at a distance z from the target that is different from the distance where the particles would cross the solenoid axis. These particles also possess flight times that are shorter than the cyclotron period. This effect is important only for inverse reactions, where the interesting particles are emitted toward backward angles near 180^o in the laboratory. These events are still readily associated with particular kinematic groups, however, and

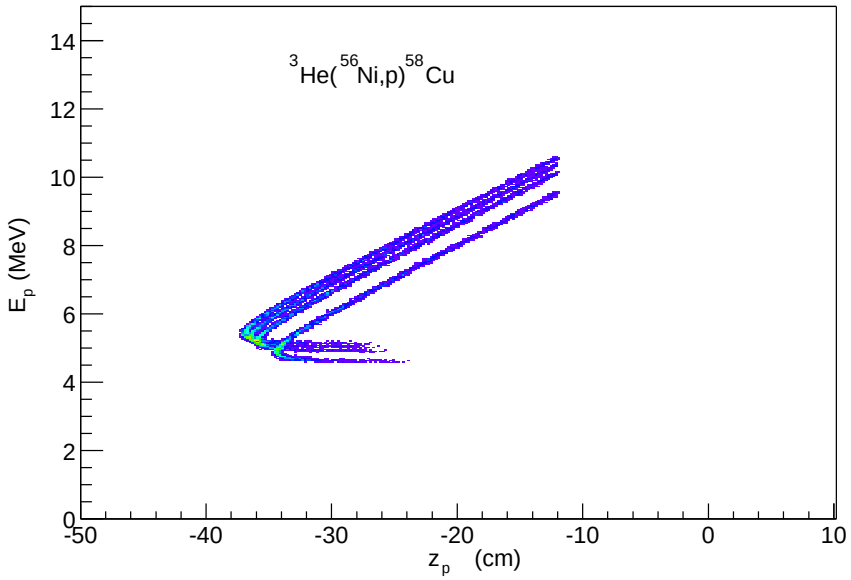

FIG. 16: Proton energy versus z_p for the ^{3}He(^{56}Ni,p)^{58}Cu reaction.

correspond to a relatively narrow range of center-of-mass angles. Here, the turn-over occurs for particles with center-of-mass angles less than approximately 10 degrees. These particles can be distinguished by their time of flight which is not equal to the cyclotron period.

The reaction Q-value is obtained as described in Appendix I, from the measured proton energy and position, and assuming a time-of-flight equal to the cyclotron period T_{cyc}. A representative Q-value spectrum appears in Fig. 4(b). The center-of-mass energy resolution is approximately equal to that of the energy resolution of the silicon detector, 50 keV FWHM. This is in contrast to the resolution of approximately 180 keV obtained if the laboratory angle and the energy of protons are used, assuming the same detector resolution and a laboratory angle resolution of 2 degrees, as illustrated in Fig. 4(a).

Using a gas target of the same thickness (1 mm) as was used at ATLAS before, the previously demonstrated beam intensity of 4×10^4/s, and an integrated cross section in the forward peak of 100-250 μb for each of the states of interest corresponds to a counting rate of 4-10 per day for each state.

2. The $^3He(^{25}Al,d)^{26}Si$ reaction

Figure 17 illustrates the kinematic curves of E_d versus θ_{lab} for deuterons from the ^{3}He(^{25}Al,d)^{26}Si reaction populating the four closely spaced levels in ^{26}Si described in Sect. II between excitation energies of 5 and 6 MeV. The most interesting angles are slightly forward of 90°. The kinematics for this reaction are similar to others where the interesting particles are emitted into the forward hemisphere such as (α, t) in inverse kinematics. For such reactions the advantages gained using the solenoid transport scheme are even more significant. In the most interesting regions, the energy versus angle kinematic loci have very large values of $dE_d/d\theta_{lab}$. In some cases, there exist two kinematic solutions corresponding to two different center-of-mass angles at the same laboratory angle. These factors make good-resolution Q-value measurements difficult with an ordinary silicon-detector array with laboratory angular resolution on the order of 1 to 2 degrees.

Figure 18 gives the dependence of deuteron energy on position from the solenoid method. Here, the target is placed at the center of the solenoid (z_{tgt}=0 cm), and the silicon array covers from z_{det}=5 to 35 cm. The magnetic field is 5 Tesla. The kinematic shift dE_d/dz is much less significant than the $dE_d/d\theta$ in Fig. 17, considering that the expected position resolution is of the order of 1 mm, FWHM. For reactions with such "forward" kinematics, where there exist two kinematic solutions for a given laboratory angle, the different solutions are translated to different z positions, removing the kinematic ambiguity. As the very shallow trajectories are not of interest, there is no difficulty associated with particles being detected at z positions very different from the distance expected for an ideal trajectory.

For the ^{3}He(^{25}Al,d)^{26}Si reaction, the kinematic shift is such that it is impossible to resolve any of the four excited states if the Q-value is calculated from the deuteron energy and angle, as shown in Fig. 7(a). From the solenoid transport, however, the states that are separated by an excitation energy greater than that of the intrinsic silicon detector resolution can be resolved, as illustrated in Fig. 7(b).

Using a gas target, the demonstrated beam intensity of 10^5/s, and an integrated cross section in the forward peak of 0.02-0.2 mb for the relatively weak states at these energies, corresponds to a counting rate of 10-100 per day for these states.

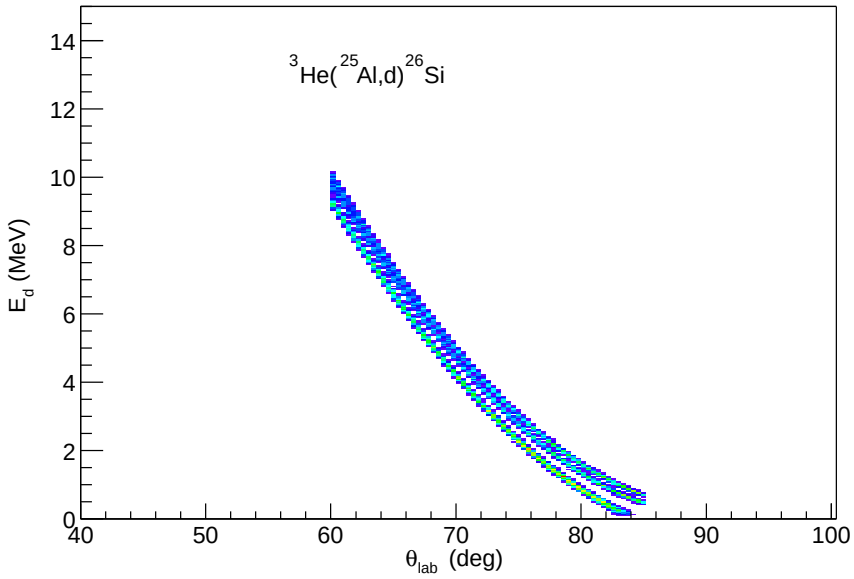

FIG. 17: Deuteron energy versus angle curves for ^{3}He(^{25}Al,d)^{26}Si at 6 MeV/nucleon.

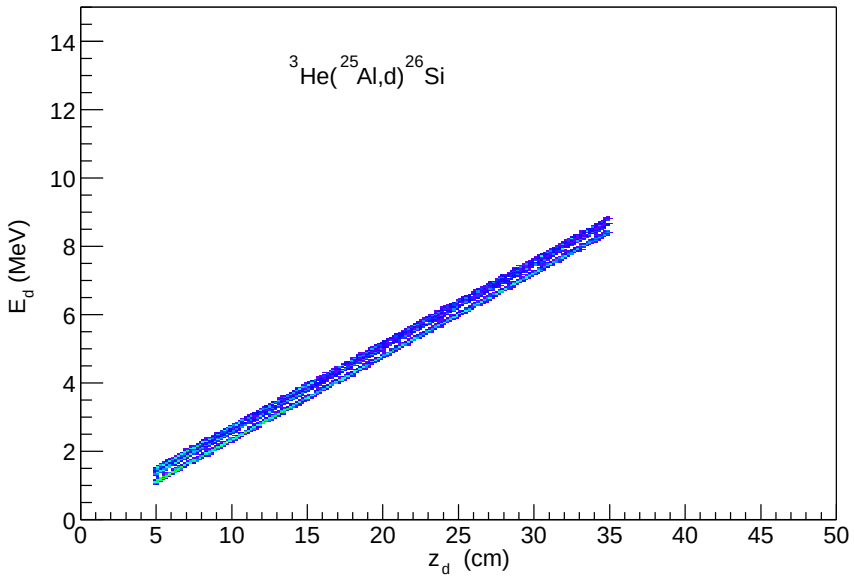

FIG. 18: Deuteron energy versus z_d curves for ^{3}He(^{25}Al,d)^{26}Si at 6 MeV/nucleon.

3. The $p(^{44}Ti,p')^{44}Ti$ reaction

Figure 19 presents the kinematic curves of proton energy versus laboratory angle for the inelastic scattering of ^{44}Ti on protons, as discussed in Sect. II. Here, the bombarding

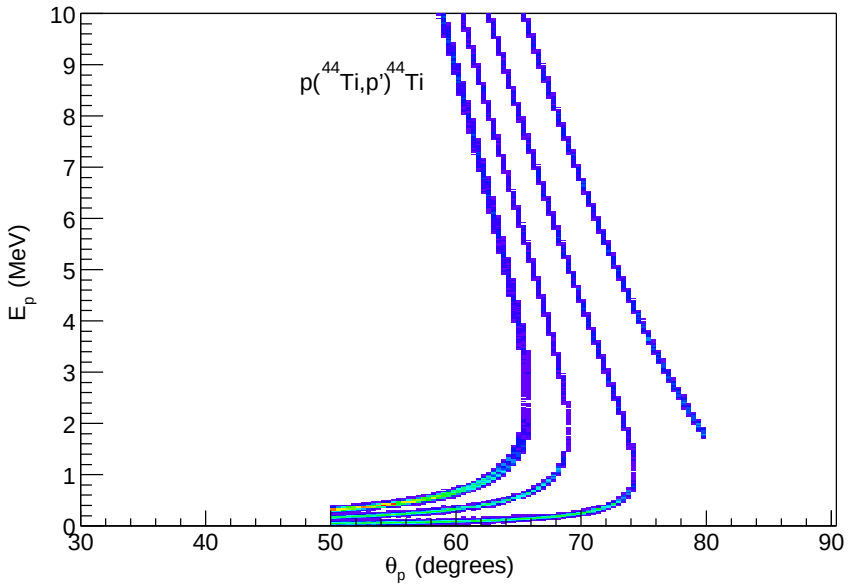

FIG. 19: Kinematic curves of proton energy versus angle for $p(^{44}\mathrm{Ti},p')^{44}\mathrm{Ti}$.

energy is 15 MeV/nucleon. These kinematics are representative of many cases where the light ejectile is emitted in the forward direction; *i.e.*, there exist large kinematic shifts, and for the most interesting angles near the maximum laboratory angle, the kinematics are double-valued, with a given laboratory angle corresponding to two possible center-of-mass angles.

This situation clearly illustrates the advantages to the solenoid technique, where the kinematic dependence of proton energy on position is a straight line, and there exists a one-to-one relationship between z position and center-of-mass angle (See Fig. 20.) The resolution in Q-value is also significantly better in the solenoid case, compared to that determined from angle and energy, as is apparent in Fig. 21.

C. Non-uniform field effects

Small non-uniformities that are axially symmetric in the magnetic field do not substantially affect the general transport properties of the solenoid. As an example, we consider a magnetic field generated by a 1.50 m long solenoid with an inner coil diameter of 0.5 m, and an outer coil diameter of 0.56 m calculated according to the prescription of *(D. Bruce Montgomery, "Solenoid magnet design", Wiley-Interscience, New York, 1969)*. For such a

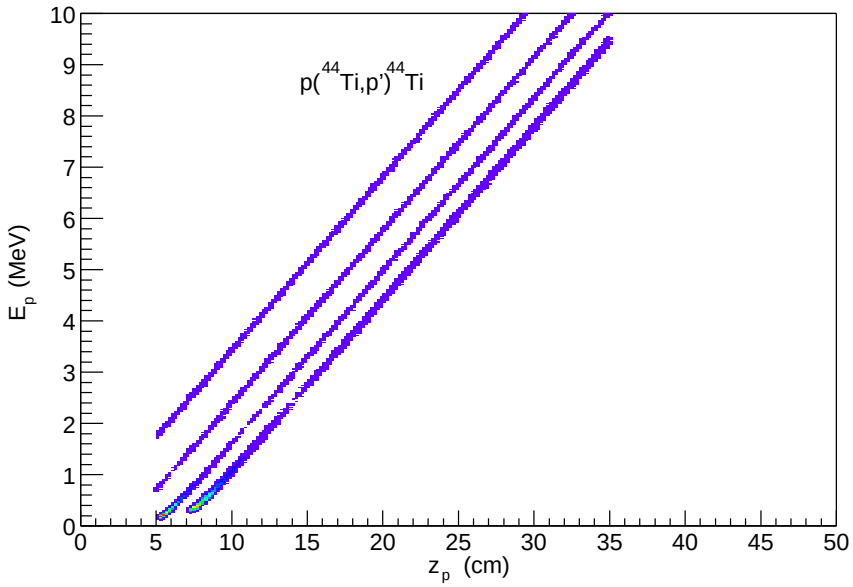

FIG. 20: Kinematic curves of proton energy versus z_p for $p(^{44}\mathrm{Ti},p')^{44}\mathrm{Ti}$.

solenoid, the greatest non-uniformities in the field are found at radii far from the target. The maximum deviations from the central axial field are of order 3% of the value at the center of the solenoid, and the maximum radial component of the field is also approximately 3% of the maximum axial field value. The effect of such non-uniformities of this type is to slightly alter the slope of E vs. z loci (see *e.g.* Fig. 16) for individual final states without affecting the Q-value resolution.

Residual, non-axially symmetric, non-uniformities in the field will depend on the accuracy with which the field coils and other field shaping materials can be manufactured and an induced field in the building. The final goal is to obtain field non-uniformities better than 10^{-3}. Since typical solenoidal magnets of this type, built for MRI applications, are specified with field non-uniformities of the order 10^{-6} in the central region, it is expected that the requirements for our application are easily met.

D. Misalignment and beam-spot size

Mechanical misalignments can play a role in the transport properties of any magnetic device. Other factors aside, the geometrical position resolution will be determined by the beam spot size and this sets a limit on the amount of misalignment that can be tolerated:

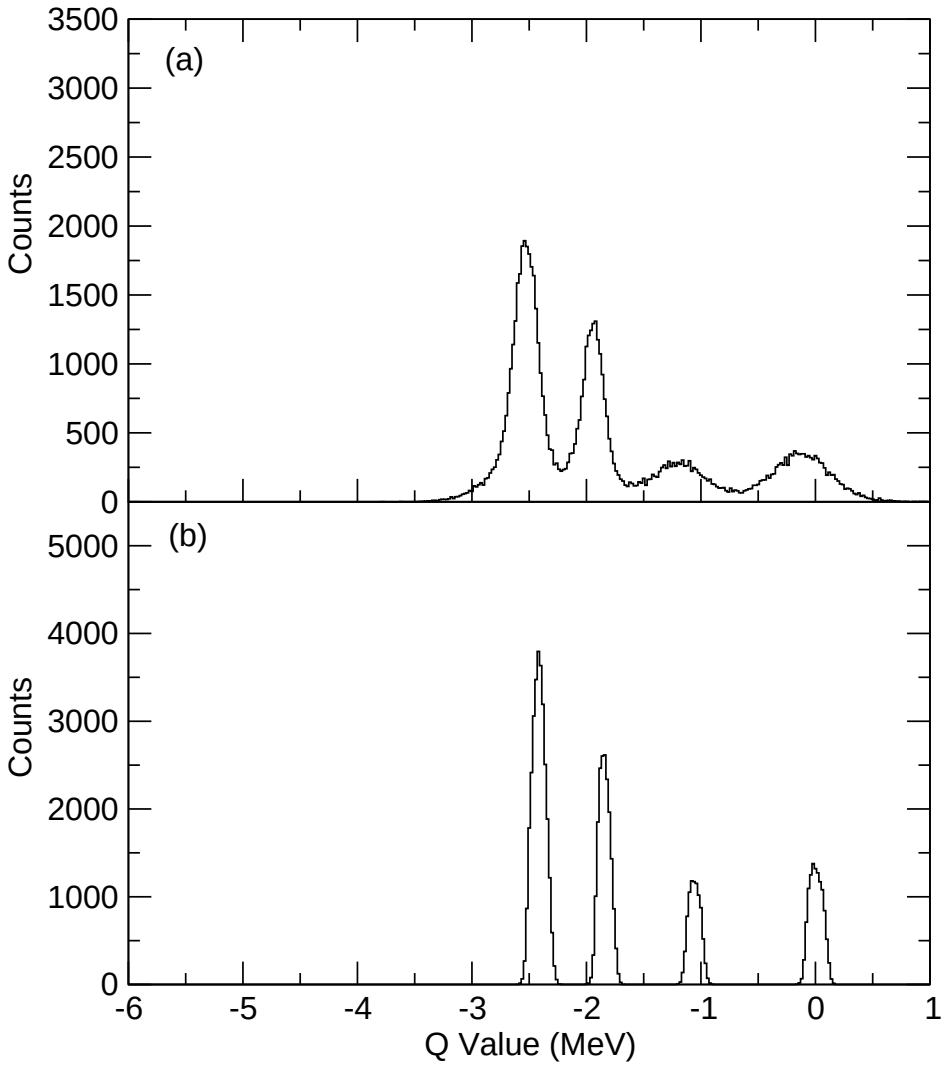

FIG. 21: Q-value spectra $p(^{44}\mathrm{Ti},p')^{44}\mathrm{Ti}$ from (a) proton energy and angle (b) proton energy and solenoid position

for a maximum target-to-detector distance of 1 m and a beam radius of 1 mm, the magnetic field should be parallel to the beam to better than 1 mrad, and the detector center should be located on the beam (magnetic) axis to better than 1 mm. Alignments of this accuracy will translate to measurements of the z position where particle trajectories impinge on the detector surface with the desired $\sim$1 mm accuracy for most trajectories, except a small region of the phase space with $\theta < 30^\circ$ or $\theta > 150^\circ$. The design of the adjustment mechanisms for the solenoid, the target wheel and detector assemblies will be such that these tolerances can be achieved.

E. Target thickness effects

The energy loss in the target will have an effect on the Q-value resolution in any reaction experiment, but especially so in inverse kinematics with heavy beams. For CH_2 and CD_2 targets, the energy loss can be significant. For example, at a bombarding energy of 6 MeV/nucleon, the energy loss for a ^{56}Ni beam in a 200 μg/cm^2 CD_2 target is approximately 7 MeV, and for a ^{132}Sn beam, the energy loss is approximately 15 MeV. This energy loss translates into a spread in the velocity of the center-of-mass system, and can degrade the Q-value resolution, regardless of the detection scheme. As a specific example, for $d(^{56}\mathrm{Ni},p)^{57}\mathrm{Ni}$ at 6 MeV/nucleon, the energy spread caused by the 200 μg/cm^2 target introduces a spread in the Q-value resolution from the solenoid spectrometer of approximately 100 keV in addition to that from the intrinsic detector resolution. In cases where the states of interest are not so closely spaced, solid targets with thicknesses of more than 200 μg/cm^2 are still desirable because of low beam intensity. For more demanding situations, however, it may be more appropriate to use windowed gas targets of H_2 or D_2 instead of polyethylene foils.

With gas targets, the effects due to target thickness are actually much less severe, as the bombarding energy is spread only by energy straggling in the entrance window of the gas cell, and by the energy loss in the gas containing the same thickness of hydrogen. Both effects are considerably smaller than the energy loss in the solid polyethelyne targets. For 6 MeV/nucleon Ni beams, for example, both straggling and energy loss are less than 1 MeV, for either hydrogen or helium isotope gas targets as compared to 6-7 MeV in a CH_2 foil. The gas target used at ANL has an effective length of approximately 1 mm, and the corresponding spread in the z position of the interaction is comparable to the assumed z resolution of the silicon detector array.

APPENDIX A: PARTICLE MOTION IN A SOLENOID

The nomenclature used in this appendix and throughout the proposal is illustrated in Fig. 22.

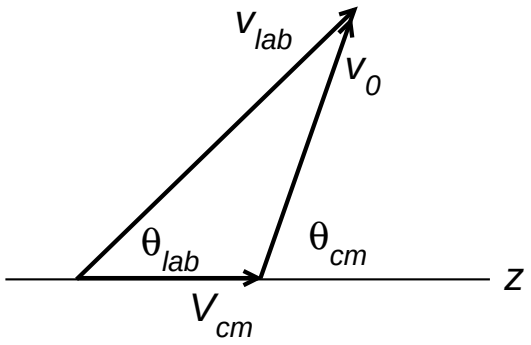

FIG. 22: The vector diagram showing the velocity of the center-of-mass system, V_{cm}, the particle velocities v_0 and v_{lab} in the center-of-mass and laboratory frames, as well as their angles θ_{cm} and θ_{lab}.

1. Transverse motion - cyclotron orbit

In a homogenous magnetic field of strength $\mathcal{B}$, a charged particle of mass m and charge qe performs a helical motion with radius r given by

$$r = \frac{mv_\perp}{qe\mathcal{B}}, \tag{A1}$$

where $v_\perp$ is the velocity of the particle perpendicular to the field lines. Note that the radius is independent of the longitudinal velocity, $v_\parallel$. The cyclotron period, *i.e.* the time for one orbital motion, is

$$T_{cyc} = \frac{2\pi r}{v_\perp} = \frac{2\pi}{\mathcal{B}}\frac{m}{qe}. \tag{A2}$$

From a measurement of the period, T_{cyc} obtained by a time-of-flight measurement, one obtains

$$\frac{m}{qe} = \frac{\mathcal{B}}{2\pi}T_{cyc}, \tag{A3}$$

i.e. the mass to charge ratio, which in most cases identifies the particle (except *e.g.* deuterons and α particles). Once the particle has been identified, one may therefore use the right

hand side of Eq. A2 to obtain an accurate value for the cyclotron period. Using this value instead of the measured value removes the experimental uncertainty from the estimates of the center-of-mass energy and scattering angle which will be derived below.

2. Longitudinal motion

The component of the velocity along the beam axis (which is assumed to be parallel to the $\mathcal{B}$-field lines) is given by

$$z = v_{\parallel} T_{cyc} = (V_{cm} + v_0 \cos\theta_{cm}) T_{cyc}, \tag{A4}$$

which may also be written

$$z = \frac{2\pi\sqrt{2mE_{lab}}}{qe\mathcal{B}} \cos\theta_{lab}. \tag{A5}$$

Note that the velocity, V_{cm}, of the center-of-mass gives rise to a constant displacement in z, with the *relative* z-values independent of this motion.

3. Energy measurement

The particle energy in the laboratory frame may be written as

$$E_{lab} = \frac{m}{2}(v_{\parallel}^2 + v_{\perp}^2) = \frac{m}{2}\left[(V_{cm} + v_0\cos\theta_{cm})^2 + v_0^2 \sin^2\theta_{cm}\right]. \tag{A6}$$

Inserting the expression for $v_0 \cos\theta_{cm}$ obtained from eq. 4 one obtains

$$E_{lab} = E_{cm}\frac{mV_{cm}z}{T_{cyc}} - \frac{m}{2}V_{cm}^2, \tag{A7}$$

or by solving for E_{cm}

$$E_{cm} = E_{lab} + \frac{m}{2}V_{cm}^2 - \frac{mV_{cm}z}{T_{cyc}}. \tag{A8}$$

Since the cyclotron period T_{cyc} is accurately determined from the particle identification and the strength of the $\mathcal{B}$-field, we find that the center-of-mass energy, E_{cm} is obtained directly from the measured laboratory energy E_{lab} after applying a correction depending on the distance z traveled along the beam axis. This latter is measured with high accuracy. From the determinations of the energy E_{lab} and the distance z for a particle one can therefore deduce the center-of-mass energy, E_{cm} and angle θ_{cm} from

$$E_{cm} = E_{lab} + \frac{m}{2}V_{cm}^2 - \frac{V_{cm}qe\mathcal{B}}{2\pi}z, \tag{A9}$$

and

$$\theta_{cm} = \arccos\left(\frac{v_0\cos\theta_{cm}}{v_0}\right) = \arccos\left(\frac{1}{2\pi}\frac{qe\mathcal{B}z - 2\pi m V_{cm}}{\sqrt{2mE_{lab} + m^2V_{cm}^2 - mV_{cm}qe\mathcal{B}z/\pi}}\right). \quad \text{(A10)}$$

4. Error propagation

Since measurements of E_{lab} and z are needed to compute the center-of-mass energy E_{cm}, the error on both of these measurements contributes to the estimate of E_{cm}, such that

$$\delta E_{cm} = \sqrt{\delta E_{lab}^2\left(\frac{dE_{cm}}{dE_{lab}}\right)^2 + \delta z^2\left(\frac{dE_{cm}}{dz}\right)^2} \quad \text{(A11)}$$

$$= \sqrt{\delta E_{lab}^2 + \delta z^2\left(\frac{V_{cm}qe\mathcal{B}}{2\pi}\right)^2}. \quad \text{(A12)}$$

5. Acceptance

The limited extend of the solenoidal field and the geometry of the Si-detector array pose limits on the acceptance region of a practical spectrometer in terms of particle energy and emission angle. The maximum excursion of the particle away from the solenoid axis, $d_{max} = 2r$, must be less than the radius of the vacuum vessel, r_{vac} and larger than the outer radius of the Si-detector array, r_{Si}. Re-writing Eq. A1 one finds

$$\frac{1}{8m}\left(\frac{r_{Si}qe\mathcal{B}}{\sin\theta_{lab}}\right)^2 \leq E_{lab}(\theta_{lab}) \leq \frac{1}{8m}\left(\frac{r_{vac}qe\mathcal{B}}{\sin\theta_{lab}}\right)^2. \quad \text{(A13)}$$

Likewise, the longitudinal extend of the Si-array reduces the acceptance. Re-writing Eq. A5, *i.e.* the longitudinal distance traveled by a particle before it returns to the axis, we find

$$\frac{1}{8\pi^2 m}\left(\frac{z_{min}qe\mathcal{B}}{\sin\theta_{lab}}\right)^2 \leq E_{lab}(\theta_{lab}) \leq \frac{1}{8\pi^2 m}\left(\frac{z_{max}qe\mathcal{B}}{\sin\theta_{lab}}\right)^2. \quad \text{(A14)}$$

The energy acceptance for protons and tritons as a function of θ_{lab} is shown in Fig. A 5 for a magnetic field strength of $\mathcal{B}$=2.5, 5 Telsa, respectively, and a specific location of a 30 long Si detector array covering the range from z_{min} to z_{max}. The values of r_{Si}= 2 cm and r_{vac} = 25 cm reflect the fact that cyclotron orbits must substantially exceed the radius of the Si detector array and remain inside the 25 cm radius vacuum vessel.

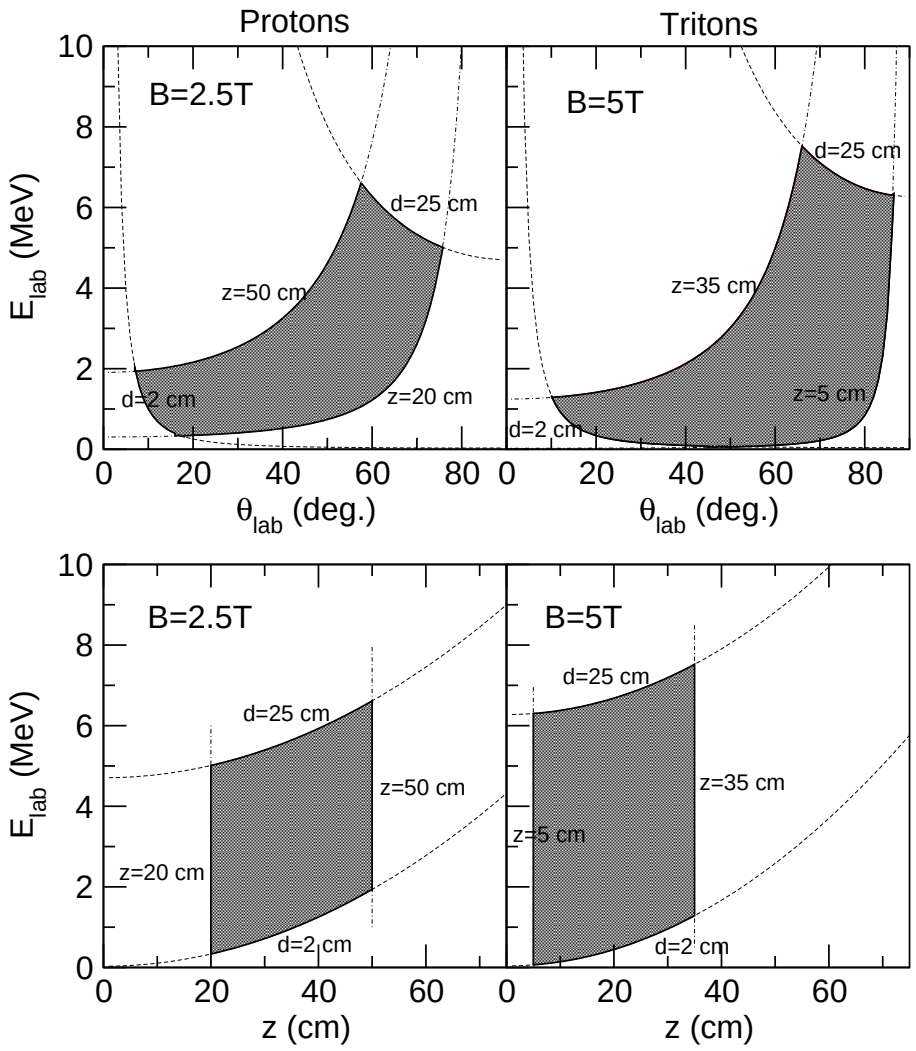

FIG. 23: This figure shows the acceptance of the spectrometer for two different configurations in magnetic field strength and position of a 30 cm long detector array. The energy acceptance for protons (left panels) and tritons (right panels) are shown as a function of laboratory angle, θ_{lab} (upper panels) and longitudinal flight distance z before returning to the solenoid axis. Individual limits imposed on the radial and longitudinal motion are indicated by dashed and dotted-dashed curves, respectively.

One may also compute the energy acceptance as a function of z by combining Eqs. A13 and A14

$$\frac{q^2e^2\mathcal{B}^2}{8m}(r_{Si}^2+\frac{z^2}{\pi^2}) \leq E_{lab}(z) \leq \frac{q^2e^2\mathcal{B}^2}{8m}(r_{vac}^2+\frac{z^2}{\pi^2}). \tag{A15}$$

The resulting acceptance limits are shown in the bottom panels of Fig. A 5.